WINTER, HEATHER LYN. Ph.D. New Leads Against Drug-Resistant Organisms: Shifting the Focus in Discovery Towards Rapid Phenotypic Screening and Mechanism of Action. (2022) Directed by Dr. Nadja B. Cech. 85 pp.

Over the past century, antibiotic therapy has been successful in nearly eliminating a former leading cause of death. Mortality records from the past 100 years in the US show a decrease from 46% of deaths due to infectious diseases, to just 3% in 2010 (1). While the use of antibiotics has had a tremendously positive impact on healthcare, the subsequent rise of antibiotic resistance in pathogens has threatened to reverse recent advances in public health and the study of antibiotic mechanisms has gained significant interest (2-5). Issues leading to emergence of antibiotic-resistant pathogens include overprescribing of antibiotics and abuses by the agricultural industry, with 50% of manufactured antibiotics used in agriculture, rather than the medical field as originally intended (6). Misuse, by failure to regard antibiotics as an inestimable resource, coupled with stagnation in discovery of new antibiotics, has led to the prevalence of antibiotic-resistant pathogens (6, 7). Approaches to combat drug resistant pathogens include large scale screening of natural sources, such as plants and fungi, for antimicrobial compounds with diverse chemical scaffolds and prioritization of antimicrobials operating by mechanisms of action which bacteria encounter infrequently.

Due to the emergence of resistance, the World Health Organization considers Gram-negative pathogen *Acinetobacter baumannii* a top priority for therapeutic development. Using this priority pathogen and a phenotypic, agar plate-based assay, a unique library of extracts from 2,500 diverse fungi was screened for antimicrobial activity against a highly virulent, drug-resistant strain of *A. baumannii* (AB5075) (8). The most potent hit from this screen was an extract from the fungi *Tolypocladium* sp., which was found to produce pyridoxatin (9, 10). Another active extract from the fungi *Trichoderma deliquescens* was characterized and yielded

Trichokonin VII and Trichokonin VIII (11). Evaluation of pyridoxatin against *A. baumannii* (AB5075) in a broth microdilution assay revealed a minimum inhibitory concentration (MIC) of 38.0 μM, which was the strongest lead compared to the known antibiotic levofloxacin MIC of 27.7 μM. Mass spectrometry, Marfey's analysis and nuclear magnetic resonance spectroscopy were utilized to confirm the structures of Trichokonin VII and Trichokonin VIII in comparison to previous reports (11). In an *in vivo Galleria mellonella* model (12, 13), pyridoxatin tested at 150 mg/kg exhibited minimal toxicity (90% survival) and promising antimicrobial efficacy (50% survival) after 5 days. Trichokonin VII and Trichokonin VIII tested at 150 mg/kg were toxic, with 20% survival and 40% survival after 5 days, respectively. The findings of this project suggest that pyridoxatin may serve as a lead compound for the development of antimicrobials against *A. baumannii*. They also demonstrate the value of the phenotypic screening approach employed here to uncover diverse lead antimicrobial compounds.

A second approach to counteracting antimicrobial resistance was taken with a botanical extract mechanism of action classification prediction method that was developed using metabolomics in the model antimicrobial system of *Hypericum calycinum* (creeping St. John's wort) against Methicillin-resistant *Staphylococcus aureus* (MRSA). Antimicrobial botanicals, such *as H. calycinum*, exhibit unique mechanisms of action due to a complex array of compounds and combination effects which challenges bacteria in developing resistance (14). MRSA strain USA300 LAC AH1263 (15), a model organism we observed with susceptibility to *H. calycinum*, is a clinically relevant drug-resistant pathogen rapidly developing resistance. To evaluate these qualities, metabolomics analyses were conducted on the spent media from MRSA cultures incubated with various treatments. The treatments included sub-minimum inhibitory concentrations (sub-MIC) of six clinically relevant antibiotics representing three mechanisms of

action. Also included in the study were a *H. calycinum* extract, an *H. calycinum* active fraction, or the pure botanical compound hyperforin commonly found in *Hypericum calycinum* (16). Previously developed metabolomics data processing techniques (17-22) were refined for evaluating profiles of the spent media and narrowing down features detected across all samples from 8,900 features to a list of 32 unique features (ions detected by the mass spectrometer) associated with mechanism of action. Further investigation of the identities of these features and biochemical studies to confirm the antimicrobial mechanism of action of *H. calycinum* against MRSA are necessary to validate the model in predicting antimicrobial mechanism of action in botanical extracts.

NEW LEADS AGAINST DRUG-RESISTANT ORGANISMS: SHIFTING THE FOCUS IN DISCOVERY TOWARDS RAPID PHENOTYPIC SCREENING AND MECHANISM OF ACTION

by

Heather Lyn Winter

A Dissertation
Submitted to
the Faculty of The Graduate School at
The University of North Carolina at Greensboro
in Partial Fulfillment
of the Requirements for the Degree
Doctor of Philosophy

Greensboro

2022

Approved by

Dr. Nadja B. Cech
Committee Chair

DEDICATION

To my daughter, Lilah. Your laughter and Grace are my inspiration every day.

APPROVAL PAGE

This dissertation written by Heather Lyn Winter has been approved by the following committee of the Faculty of The Graduate School at The University of North Carolina at Greensboro.

Committee Chair

Dr. Nadja B. Cech

Committee Members

Dr. Nicholas Oberlies

Dr. Sherri McFarland

Dr. Cedric Pearce

Dr. Daniel Todd

October 21, 2022

Date of Acceptance by Committee

October 21, 2022

Date of Final Oral Examination

ACKNOWLEDGEMENTS

Thank you Dr. Nadja Cech, my mentor, for being an unwavering leader and role model since the day we met. For always believing in me and my ideas and giving me the welcoming space, resources and support to flourish both in research and my personal life.

Thank you, Dr. Nicholas Oberlies, for supporting me from my first phone call to UNCG and pushing me throughout my studies to strive to better myself daily. Thank you for also bringing a piano to the department lobby, which has been an incredible creative outlet between experiments.

Thank you, Dr. Sherri McFarland, for your kindness, for many refreshing visits to your horse farm and sharing much needed breaths of fresh air.

Thank you, Dr. Cedric Pearce, for encouraging my passions for reading and writing, delivering many thoughtfully highlighted journal copies to help me broaden my literature knowledge.

Thank you, Dr. Daniel Todd, for unending support, teaching and talking me through my countless mass spectrometry questions.

Thank you, Dr. Lindsay Caesar, for being a role model and sharing your inspiring and unique ideas and perspectives. You are a mind-opening individual and have followed your footsteps along the way.

Thank you, Dr. Emily Britton, for supporting and connecting with me as a friend and role model and helping me navigate so many aspects of my future career.

Thank you, Dr. Josh Kellogg, for sharing your ethnobotanical roots, data analysis methods, and overflowing excitement for researching in our field.

Thank you, Dr. Warren Vidar for our many walks and talks to the coffee shop. For being a one-of-a-kind friend and for above and beyond support as a lab mate.

Thank you, Fridah Rotich, for cooking with me and growing alongside me over many years, from new researchers all the way to motherhood.

Thank you, Zoie Bunch, for listening to my country music, playing piano duets with me on our breaks, jinxes, and many smiles in between.

We thank Dr. Huzefa Raja for growing fungal cultures for these studies and sequencing fungal strains for identification.

We thank Dr. Tyler Graf for training and assistance troubleshooting equipment, as well as insight on these studies.

We thank Dr. Alexander Horswill for providing *Acinetobacter baumannii* strains utilized for these studies.

We thank Dr. Christian Melander for training in techniques to perform *Galleria mellonella* cytotoxicity screening.

We thank Blaise Darvaeux of Mycosynthetix for preparing 2,500 fungal extracts from their library.

We thank you, Dr. Cody Earp, from UNCG for helpful suggestions.

This research was supported by the National Center for Complementary and Integrative Health of the National Institutes of Health under award numbers 5 T32 AT008938 and 1 F31 AT011152-01A1.

Mass spectrometry analyses were conducted in the Triad Mass Spectrometry Facility at the University of North Carolina.

TABLE OF CONTENTS

LIST OF TABLES

LIST OF FIGURES

CHAPTER I: WHAT WAS OLD IS NEW AGAIN: PHENOTYPIC SCREENING OF A UNIQUE FUNGAL LIBRARY YEILDS PYRIDOXATIN A PROMISING LEAD AGAINST EXTENSIVELY RESISTANT *ACINETOBACTER BAUMANNII* (AB5075)

Winter, H.L. wrote all sections of this manuscript except for the sections, "Fungal Strains" and "Fungal strain identification" which were written by Raja, H.A. Winter, H.L. created all of the figures except for **Fig.** 1.18 and **Fig.** 1.19 which were compiled by Raja, H.A. Cech, N.B. provided suggestions and edits throughout preparation of this manuscript.

INTRODUCTION

Routine administration of antibiotics in medical practice since the 1940s has drastically minimized the perceived threat posed by bacterial infections (23). Infections that are inconsequential with access to modern treatments accounted for 46% of all deaths in the early 1900s (1, 24). Though the use of antibiotics has had a tremendously positive impact on healthcare, failure to regard antibiotics as an inestimable resource, coupled with stagnation in development of new antibiotics, has led to the prevalence of antibiotic-resistant pathogens (6, 7). The rise of such pathogens has threatened to reverse our advancements in public health. Treatment of antibiotic-resistant infections now relies heavily upon last resort treatments (25, 26). Opportunistic antibiotic-resistant pathogens add further concern in the face of the COVID-19 pandemic, with the rise of critically ill COVID-19 patients being vulnerable to secondary antibiotic-resistant bacterial infections (26, 27). Generation of new approaches to treatment is critical to overcome antibiotic-resistant infections and prevent regression of our medical capabilities to that of the previous century.

Amongst the rapidly evolving multidrug-resistant pathogens, the Centers for Disease Control and Prevention and World Health Organization consider the Gram-negative bacterium *Acinetobacter baumannii* an urgent health risk (28, 29). An opportunistic pathogen, *A. baumannii* is particularly challenging to treat due to rapid conferral of new resistance mechanisms, with several strains demonstrating resistance to nearly all classes of antibiotics (30). To overcome antibiotic resistance in *A. baumannii*, design and discovery of alternative treatment methods is critically needed. The goal of this project was to help address this gap by identifying new antimicrobial leads against *A. baumannii*.

In efforts to develop new antimicrobial therapies, it is worthwhile to consider what strategies have led to previous successes. Most antibiotics used today were discovered between the 1940's and 1960's, a period often referred to as the antibiotic "golden age." By in large, these antibiotics were discovered by testing extracts from natural origin (from bacteria or fungi) in phenotypic screens as early as the 1930's (31). Starting in about the 1980s, drug discovery efforts began to focus more on the use of target-based screens, often employing enzyme-based assays (32). In the ensuing decade, natural product drug discovery programs based on phenotypic screens were phased out by many pharmaceutical companies. Despite this, a look at drug discovery successes in the more recent past demonstrates that phenotypic screening continued to yield positive results. For example, an analysis in *Nature Reviews* reported eleven small molecule new chemical entities approved by the FDA for treatment of infectious disease between 1999 and 2008, five of which were derived from natural sources (33). Of the eleven new chemical entities, eight were identified by phenotypic screening and only three from target-based screens. This track record of success suggests that continued efforts towards phenotypic screening are warranted, and we chose to take the phenotypic screening approach in this study.

One of the limitations that often hampers modern antibiotic discovery is the limited quality and diversity of libraries subjected to screening efforts. With this work, we were fortunate to have access to a unique library of genetically diverse fungi from the Mycosynthetix library of more than 55,000 living fungal cultures. At the time of its creation, the diversity of this collection was maximized by sampling different substrates and ecosystems. For the study described herein, we selected 2,500 fungi from the Mycosynthetix library based on prior results suggesting the promise of these organisms for producing antimicrobial compounds. We screened these extracts in a plate-based assay against a clinically relevant, extensively drug-resistant strain of *A. baumannii* (AB5075), with the goal of identifying leads that could be advanced to *in vivo* screening in a wax worm (*Galleria mellonella*) model.

RESULTS

Qualitative Antimicrobial Screening and Lead Prioritization

Fig. 1.1 Prioritization of fungal extracts by antimicrobial activity.

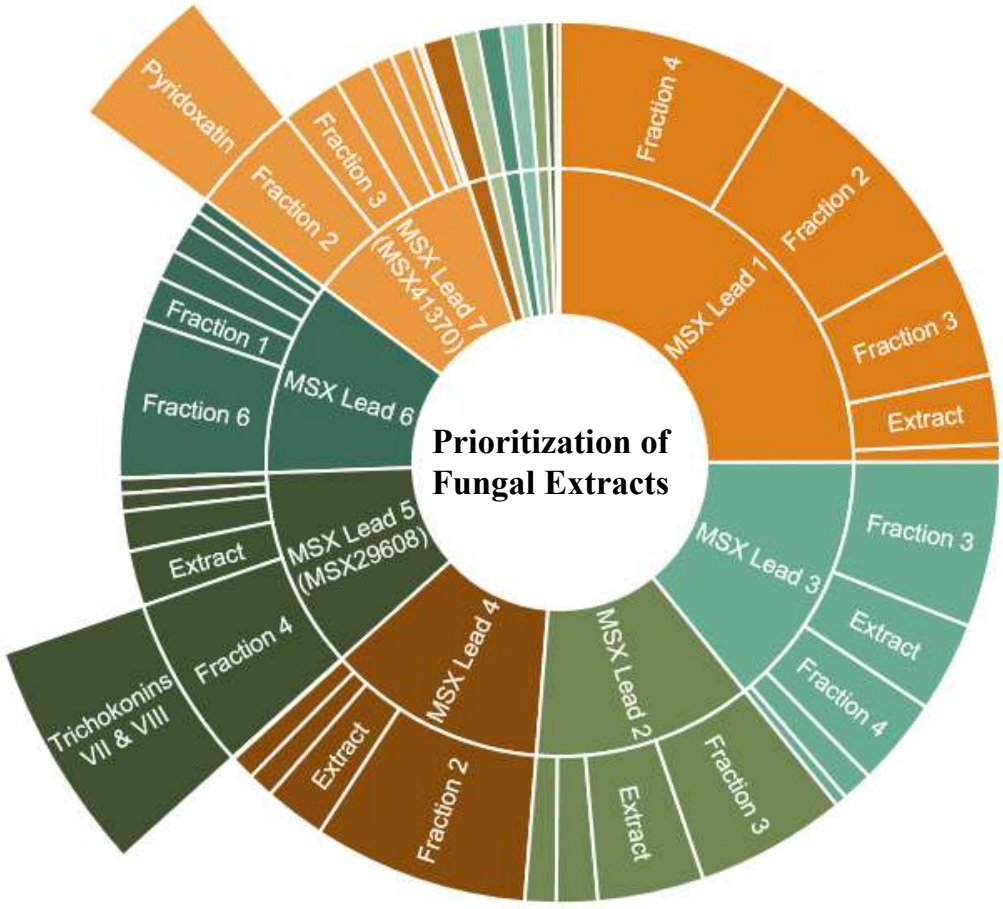

Notes. Rapid, qualitative antimicrobial screening of 2,500 Mycosynthetix (MSX) fungal extracts revealed activity of 18 lead extracts against *A. baumannii* (AB5075). Follow-up quantitative antimicrobial evaluation gave priority to 7 extracts for further chemical profiling.

From the 2,500 extracts screened, 18 extracts (**Fig.** 1.1) demonstrated inhibition zones against *A. baumannii* in the qualitative, plate-based assay (**Fig.** 1.2).

Fig. 1.2 (A-F) Antimicrobial agar dish screening assay for 2,500 MSX fungal extracts against *A. baumannii* (AB5075).

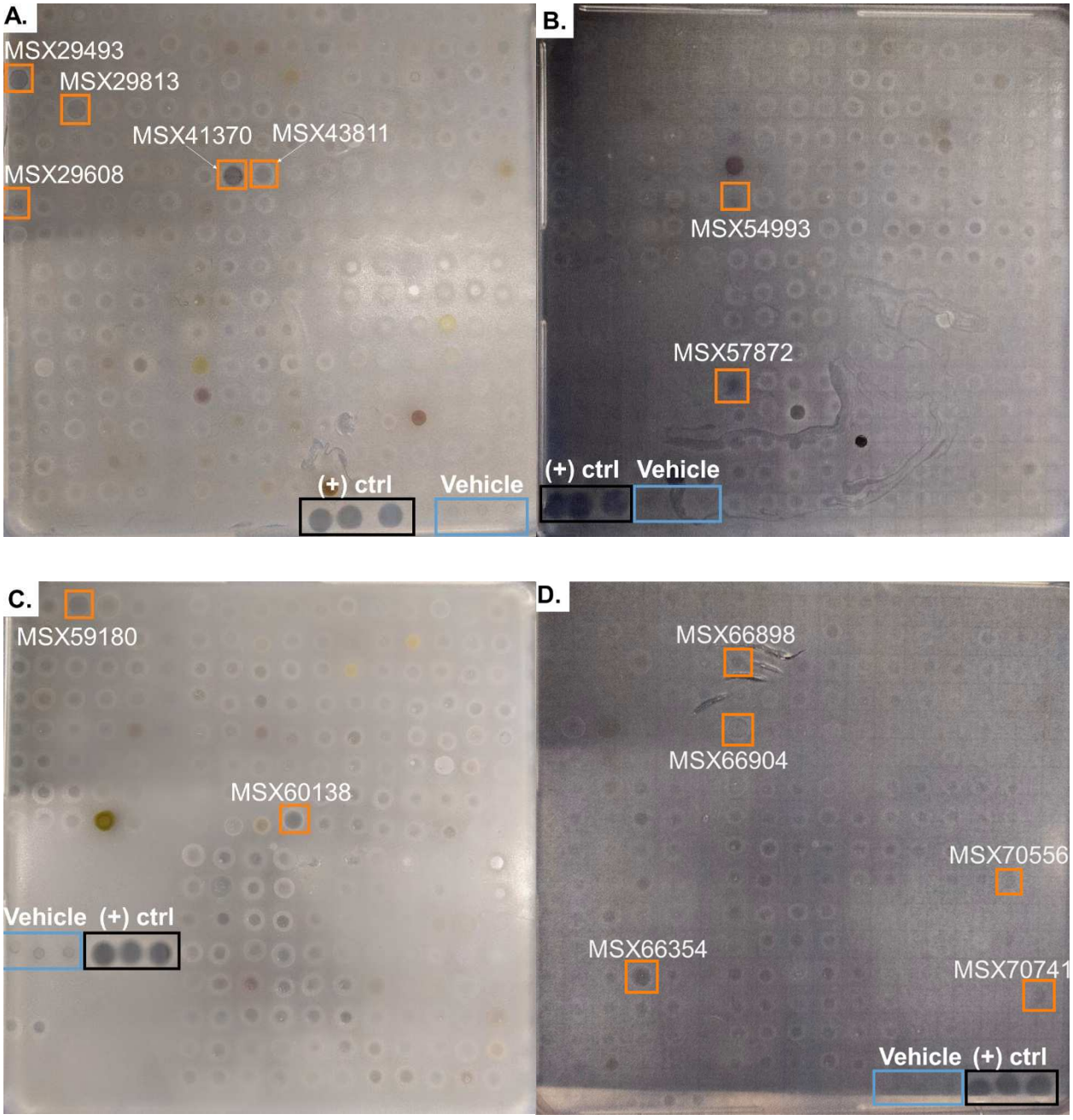

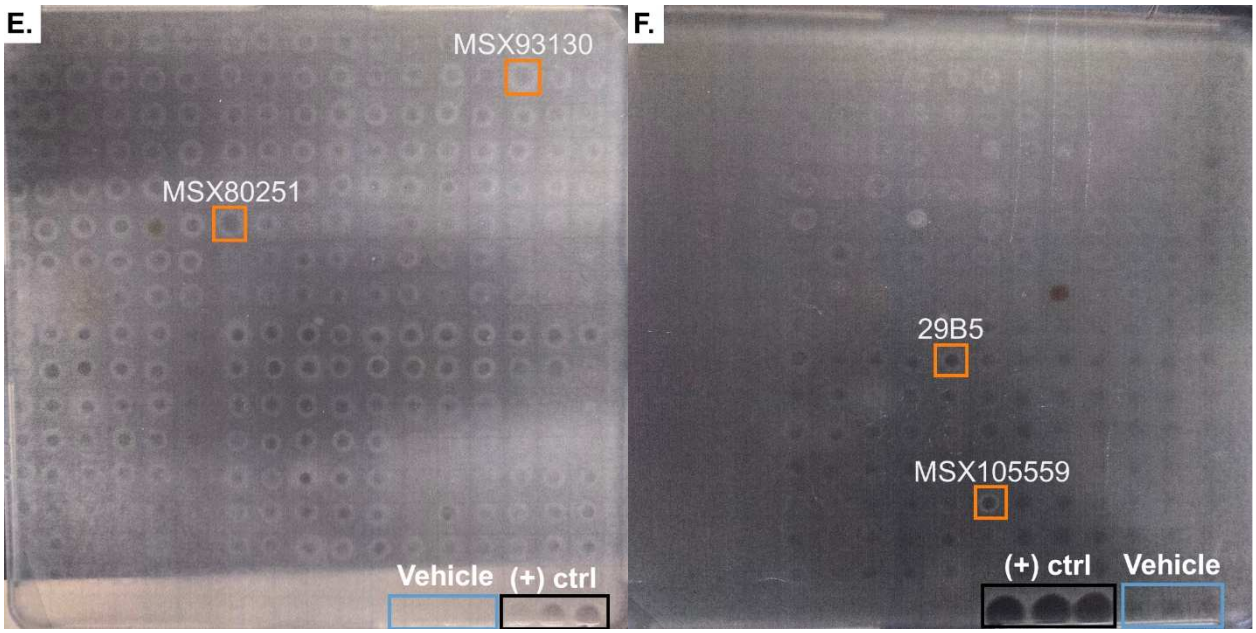

Notes. In panels A-F, antimicrobial dishes with qualitative inhibitory activity are annotated. MSX fungal extracts in neat DMSO were uniformly spotted in 5 µL aliquots, where orange boxes indicate inhibition by 5 µL of MSX fungal extracts qualitatively identified as active. Blue boxes indicate triplicate control of vehicle (5 µL of neat DMSO). Black boxes indicate positive control (5 µL of 2.77 mM levofloxacin in neat DMSO).

Cultures of the fungi that had produced active extracts in the initial screening were regrown and fractionated into a peak library using previously described approaches (34). The extracts and fractions were tested in a quantitative broth microdilution assay according to Clinical Laboratory Standards Institutes (CLSI) guidelines (**Fig.** 1.1) (34, 35). Eleven of the regrown extracts were inactive in the quantitative assay and were not pursued, but seven showed promising activity (**Fig.** 1.3).

Fig. 1.3 Quantitative antimicrobial 96-well assay of large-scale regrown cultures of 18 lead extracts and derived fractions against *A. baumannii* (AB5075).

MSX ID	Extract	Fraction 1	Fraction 2	Fraction 3	Fraction 4	Fraction 5	Fraction 6	Fraction 7
29813	28.26	7.12	93.85	52.63	95.42			
93130	43.37	12.71	16.82	61.50				
29493	36.76	4.78	12.55	67.50	36.07			
80251	24.98	9.99	87.73	0.73	10.46			
29608	22.46	7.24	6.08	0.17	71.05			
66898	16.25	18.21	6.72	12.30	5.61	11.72	64.37	
41370	3.03	0.00	15.51	46.16	24.71	1.69	8.68	8.93
54993	7.66	8.04	8.46	28.99				
60138	9.69	18.44	20.81	6.61	4.60			
57872	12.62	3.60	5.17	19.51	10.10			
43811	4.06	2.87	0.33	22.42	6.25			
66354	9.94	5.31	10.19	6.25	0.97	0.25		
66904	2.30	12.82	4.01	-3.56				
59180	-2.47	0.00	6.80	10.53	4.45			
70741	10.01	9.57	0.43	-3.71	-1.43			
70556	-0.84	11.43	3.54	0.26	-0.13			
105559	-3.79	8.33	0.49		3.12			
29B5								

Notes. Data shown as % inhibition referenced against vehicle control.

The active extracts and fractions were analyzed by high resolution mass spectrometry and the data obtained (accurate mass, retention time, and fragmentation pattern) were compared against a database of known fungal secondary metabolites to putatively identify active constituents of the extracts as described previously (36, 37).

Identification of Extract Constituents

Examination of the mass spectrometry data for the 7 active extracts revealed the presence of several known compounds (**Fig.** 1.4). Pyridoxatin was identified in MSX41370. Extract MSX80251 contained verticillin D, which is representative of a class containing compounds

known to have cytotoxicity (38), thus, this extract was not pursued further. Mass spectral data of the remaining five extracts suggested the presence of peptides of the peptaibol class. An extract from fungus MSX29608 was chosen as a representative of these extracts for further study.

Fig. 1.4 Summary of MS base peak chromatograms of 7 lead MSX fungal extracts demonstrating antimicrobial activity against *A. baumannii* (AB5075).

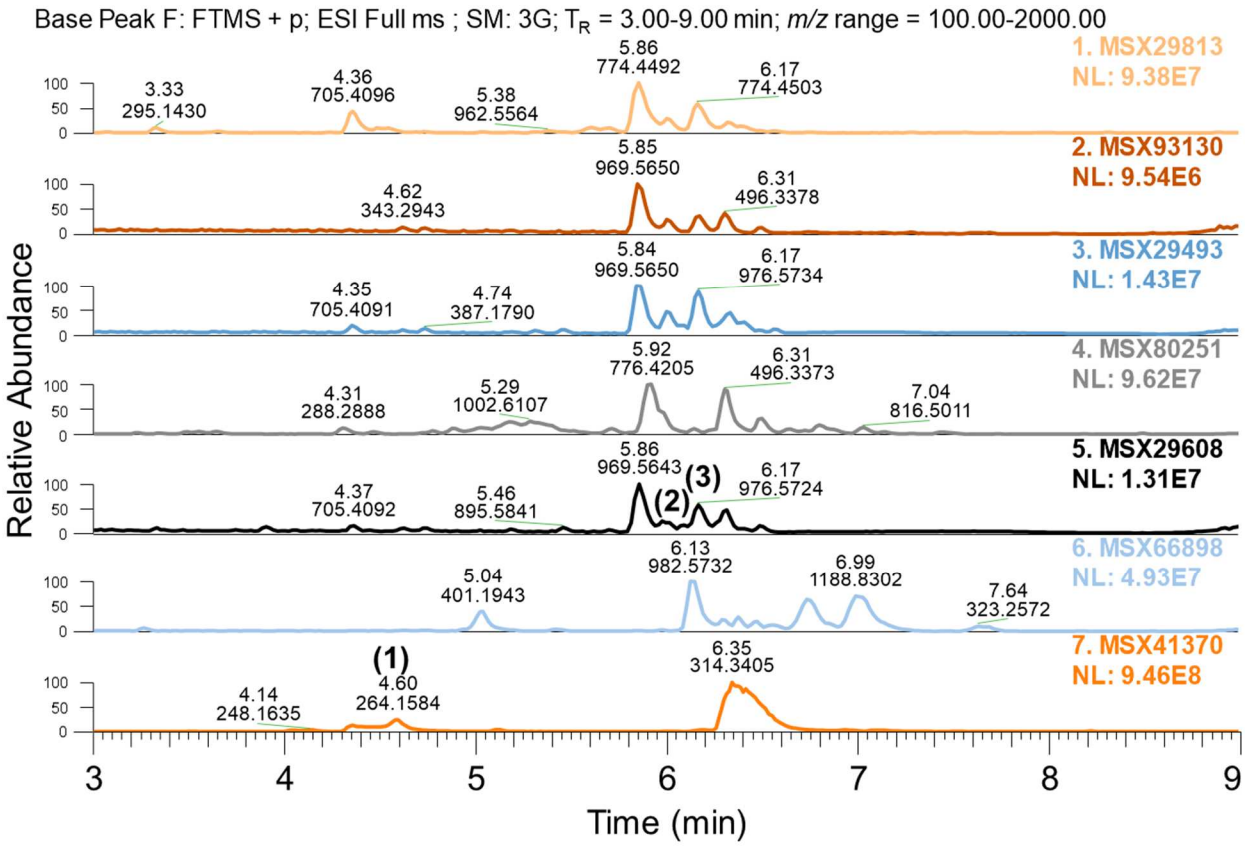

Notes. Pyridoxatin, Trichokonin VII and Trichokonin VIII are highlighted as 1, 2 and 3 respectively. Data were compared to a vehicle control (methanol) and collected using a chromatography and instrument method designed for in-house compound dereplication on a Thermo Fisher Scientific LTQ Orbitrap XL with positive mode electrospray ionization (ESI) coupled to a Waters Acquity UHPLC column (BEH C18, 1.7 µm, 2.1 × 50 mm, Waters Corporation, Milford, MA, USA).

Structural Characterization

Pyridoxatin

The extract of fungus MSX41370 was found to contain rotamers of the known compound pyridoxatin. These rotamers continuously interconvert due to a rotating stereocenter connecting both ring systems, extending along the C-7 to C-3 axis (Fig. 1.5) (39). They are not separable. The identity of pyridoxatin in the extract was confirmed by comparison of mass spectrometry data to compounds previously isolated in-house and catalogued in a mass-spectrometry database containing accurate mass, retention time and fragmentation patterns, and comparison to a purchased standard of pyridoxatin (AdipoGen Life Sciences, ≥99.6% purity) (**Fig.** 1.5**, Fig.** 1.6**,** Table 1.1) (36, 37).

Fig. 1.5 Structural rotamers of pyridoxatin ($C_{15}H_{21}NO_3$).

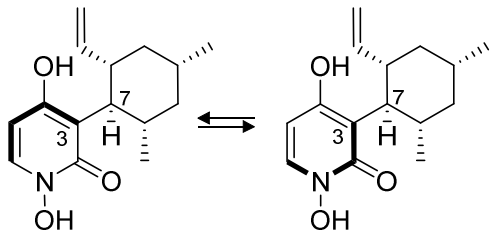

Pyridoxatin

Notes. Shown as previously reported and confirmed by comparison to an in-house mass-spectrometry database and to a purchased standard (AdipoGen Life Sciences, ≥99.6% purity) by accurate mass, retention time, and fragmentation pattern (10, 40).

Table 1.1. Pyridoxatin comparison of purchased standard to fungal extract of MSX41370.

	Standard pyridoxatin (major; minor)	MSX41370 (major; minor)
$[M + H]^+$, *m/z*	264.1585; 264.1587	264.1584; 264.1584
Retention Time, minutes	4.58; 4.39	4.60; 4.36
MS/MS Fragments, *m/z*	139.9706, 154.0180, 168.0438, 182.0600, 208.1227, 222.2133; 139.9778, 154.0053, 168.0354, 182.0678, 208.1944, 222.1110	139.9447, 153.9581,168.0186, 181.9708, 208.0475, 222.1526; 139.9773, 153.9651, 167.9749, 182.0111, 208.0994, 222.1099

Notes. Analytical UHPLC-MS data were collected on a Thermo Fisher Scientific LTQ Orbitrap XL with positive mode electrospray ionization (ESI) coupled to a Waters Acquity UHPLC column (BEH C18, 1.7 µm, 2.1 × 50 mm, Waters Corporation, Milford, MA, USA). Fragmentation data of the extract and standard were collected with collision induced dissociation (CID, 30 eV, 35 eV respectively).

Fig. 1.6 (A-C) Base peak chromatogram of pyridoxatin in the extract from MSX41370 in panel A (green) and the analytical standard (black).

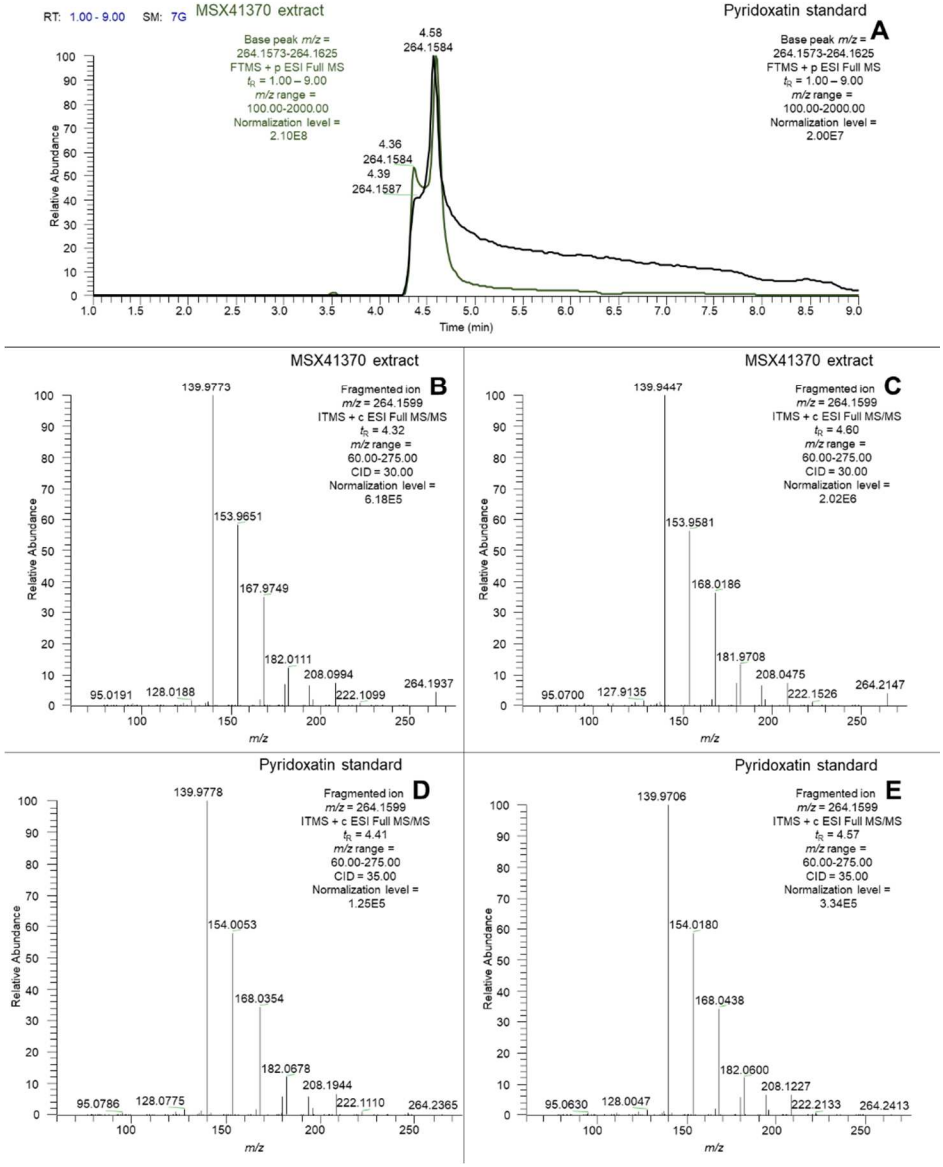

Notes. The molecular formula of pyridoxatin $[M + H]^+$, $C_{15}H_{22}NO_3$, and *m/z* = 264.1584 observed in both peaks of the extract, Δ = 0.4, 1.1 ppm compared to the standard. Shown are the MS/MS fragmentation pattern of pyridoxatin in MSX41370 (panels B and C) and MS/MS fragmentation pattern of the analytical standard of pyridoxatin (panels D and E). Data were collected on a Thermo Fisher Scientific LTQ Orbitrap XL with positive mode electrospray ionization (ESI) coupled to a Waters Acquity UHPLC column (BEH C18, 1.7 µm, 2.1 × 50 mm, Waters Corporation, Milford, MA, USA). Fragmentation data were collected with collision induced dissociation (CID, 30 eV, 35 eV respectively).

Dual peaks signature of the two rotamers were observed in the base peak chromatogram obtained by analysis of the extract (**Fig.** 1.6 **A**), and the mass spectra associated with these peaks showed a signal at *m/z* = 264.1584 $[M + H]^+$ (calculated $C_{15}H_{22}NO_3$ *m/z* = 264.1599), each with the same fragmentation patterns (**Fig.** 1.6 **B-C**). Fragmentaton patterns for the putative pyridoxatin peaks in the extract matched those obtained for a pyridoxatin standard (**Fig.** 1.6 **D-E**). Isolation of pyridoxatin from the extract was not pursued for these studies and a purchased standard of pyridoxatin was used for all *in vivo* and *in vitro* experiments.

Trichokonin VII and Trichokonin VIII

Fig. 1.7 Structures of Trichokonin VII ($C_{91}H_{151}N_{23}O_{24}$) and Trichokonin VIII ($C_{91}H_{151}N_{23}O_{24}$).

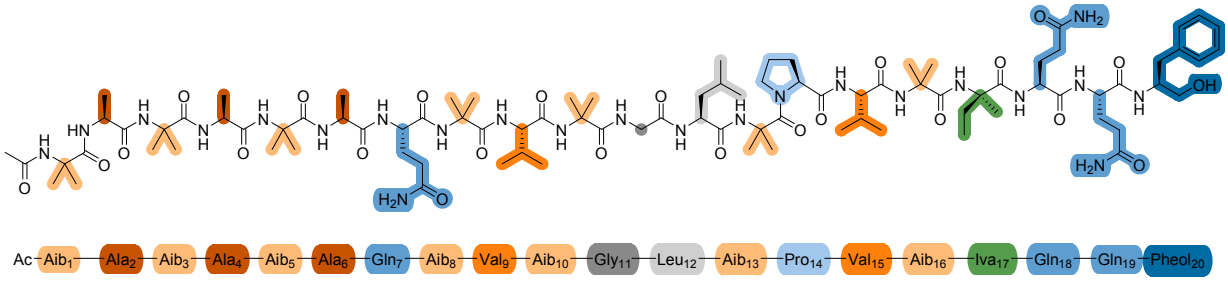

(2) Trichokonin VII

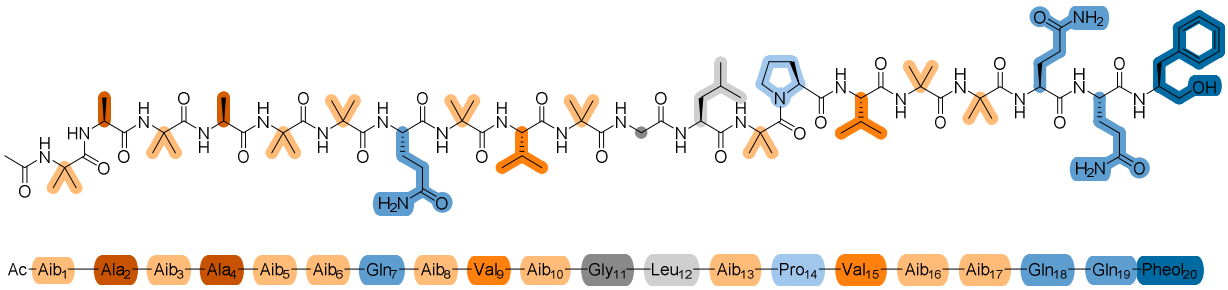

(3) Trichokonin VIII

Notes. Structures are consistent with previously reported literature (41).

Structural elucidation was carried out for the amino acid sequences and absolute configurations of Trichokonin VII and Trichokonin VIII from an extract of the fungus MSX29608 utilizing high-resolution mass spectrometry (MS and tandem MS/MS analyses), nuclear magnetic resonance (NMR) consisting of experiments in 1D (^{1}H NMR and ^{13}C and Marfey's analyses (Fig. 1.7). Mass spectral data indicated the presence of multiple adducts, in-source fragments, and MS/MS fragments of Trichokonin VII and Trichokonin VIII, observed *m/z* = 1951.1405 $[M+H]^+$ (calculated $C_{91}H_{152}N_{23}O_{24}$ *m/z* = 1951.1378) and observed *m/z* = 1951.1393 $[M+H]^+$ (calculated $C_{91}H_{152}N_{23}O_{24}$ *m/z* = 1951.1378), respectively (

Fig. 1.8-**Fig.** 1.13**)**.

Adducts observed were *m/z* = 1951.1405 $[M + H]^+$, 976.0765 $[M + 2H]^{2+}$, 984.5887 $[M + H+ NH_4]^{2+}$, 651.3870 $[M + 3H]^{3+}$ and 1301.4330 $[2M + 3H]^{3+}$ (

Fig. 1.8**, Fig.** 1.11). Two defining in-source fragments distinguish Trichokonin VII: 788.4694 y_7^+, 1163.6829 b_{13}^+ (

Fig. 1.8) and Trichokonin VIII: 774.4534 y_7^+, 1177.6980 b_{13}^+ (**Fig.** 1.11). Comparison to previously reported tables of spectral data was found to have a high degree of overlap and all expected fragments for the sequential loss of each of the 20 amino acids in Trichokonin VII **(Fig.** 1.9**-Fig.** 1.10) and Trichokonin VIII (**Fig.** 1.12**-Fig.** 1.13) were observed (**Table 1.2**).

1D NMR data were collected and matched to literature reports to confirm amino acid sequences (**Fig.** 1.14**-Fig.** 1.15**)** (41).

Fig. 1.8 Trichokonin VII ($C_{91}H_{151}N_{23}O_{24}$) analyzed with LC-MS from sample MSX29608-01077-126-1.

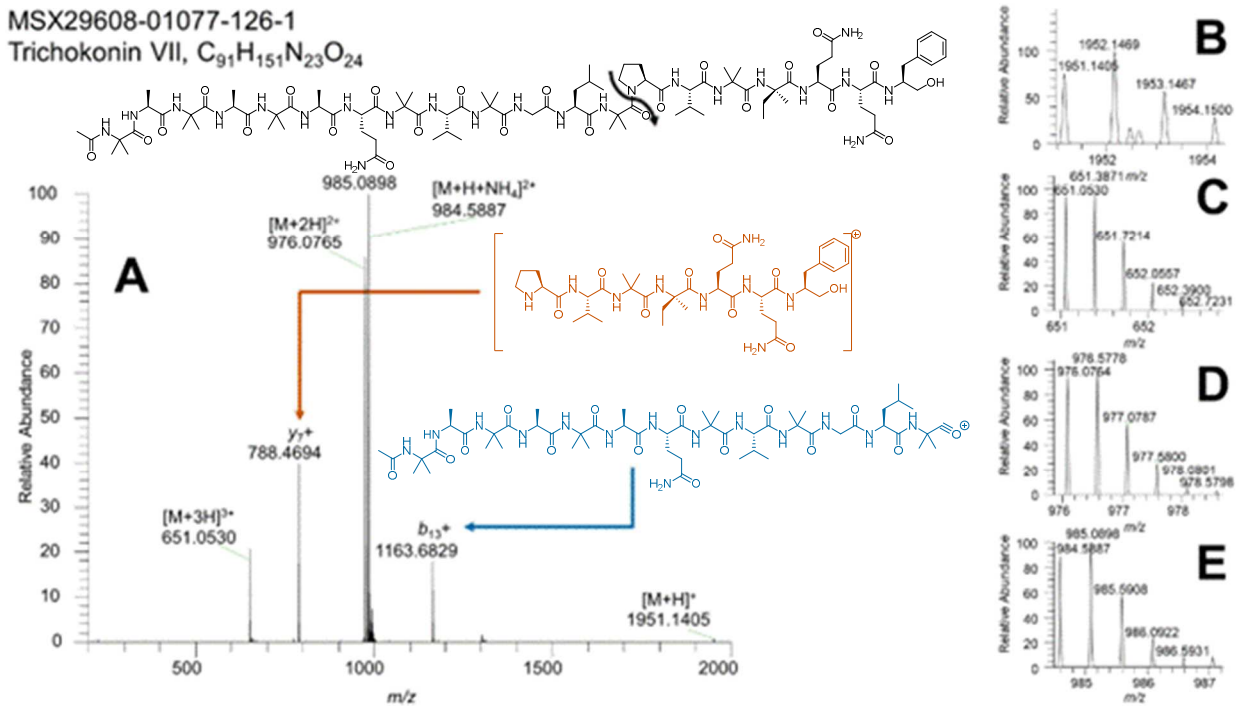

Notes. Panel A shows the full scan spectrum with diagnostic ions for Trichokonin VII annotated. Primary in-source fragments y_7^+ and b_{13}^+ are highlighted with representative structures. Panels B-E show zoomed-in regions for the labeled adducts from panel A. Signature ions include *m/z* = 1951.1405 $[M + H]^+$, 984.5887 $[M + H + NH_4]^{2+}$, 985.0898 (base peak) ^{13}C $[M + H + NH_4]^{2+}$, 976.0765 $[M + 2H]^{2+}$, 651.0530 $[M + 3H]^{3+}$, 788.4694 y_7^+, 1163.6829 b_{13}^+. Data were collected on a Thermo Fisher Scientific Q-Exactive Plus Orbitrap mass spectrometer with positive mode electrospray ionization (ESI) coupled to a Waters Acquity UHPLC column (BEH C18, 1.7 µm, 2.1 × 50 mm, Waters Corporation, Milford, MA, USA).

Fig. 1.9 Trichokonin VII MS/MS from sample MSX29608-01077-126-1 of precursor ions *m/z* = 1301.7662 and *m/z* = 976.5782 at t_R = 5.95 min.

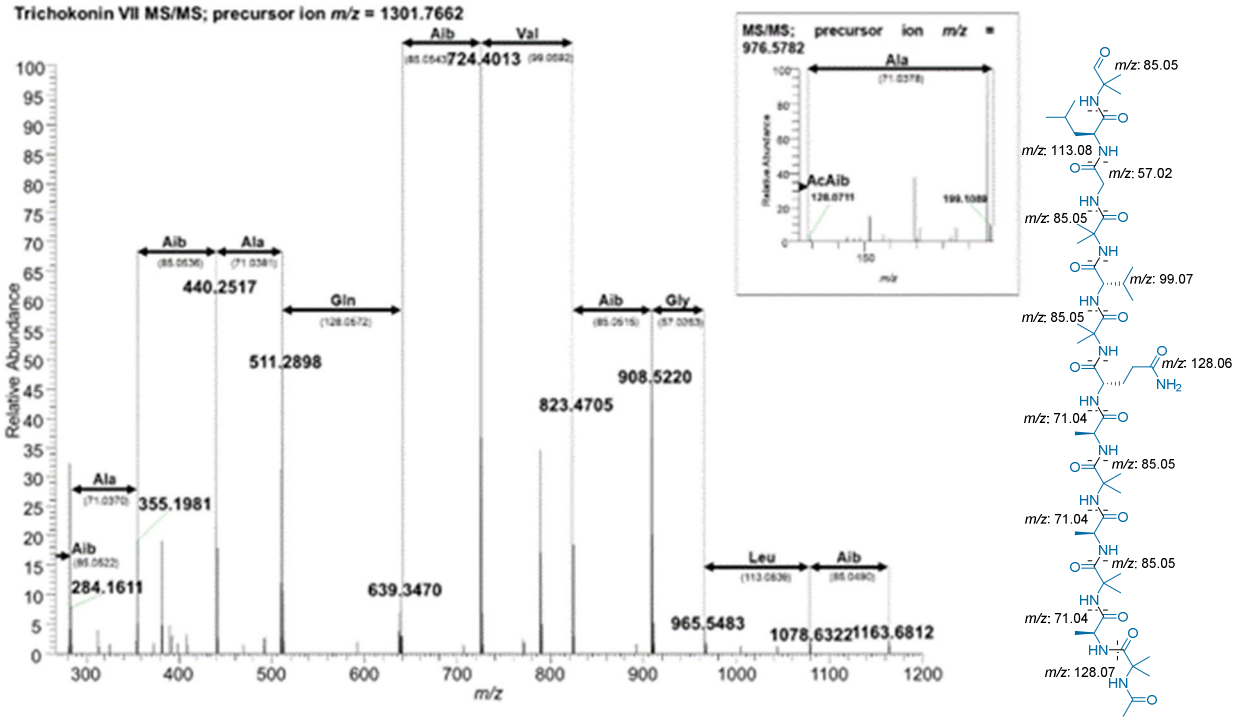

Notes. Fragmented amino acids are identified for the *b* positions of the peptaibol. The full sequence of Trichokonin VII was determined matching literature as Ac-Aib[1]-L-Ala[2]-Aib[3]-L-Ala[4]-Aib[5]-L-Ala[6]-L-Gln[7]-Aib[8]-L-Val[9]-Aib[10]-Gly[11]-L-Leu[12]-Aib[13]-L-Pro[14]-L-Val[15]-Aib[16]-D-Iva[17]-L-Gln[18]-L-Gln[19]-L-Pheol[20]. Predicted fragmentation patterns and theoretical *m/z* values were generated in ChemDraw Professional v. 21.0.0.28. Data were collected on a Thermo Fisher Scientific Q-Exactive Plus Orbitrap mass spectrometer with positive mode electrospray ionization (ESI) coupled to a Waters Acquity UHPLC column (BEH C18, 1.7 µm, 2.1 × 50 mm, Waters Corporation, Milford, MA, USA). Fragmentation data of Trichokonin VII were collected with a normalized collision energy of 30 eV for the high-energy collision-induced dissociation (HCD).

Fig. 1.10 Trichokonin VII MS/MS from sample MSX29608-01077-126-1 of y^{7+} precursor ion *m/z* = 788.4697 at retention time t_R = 5.93 min.

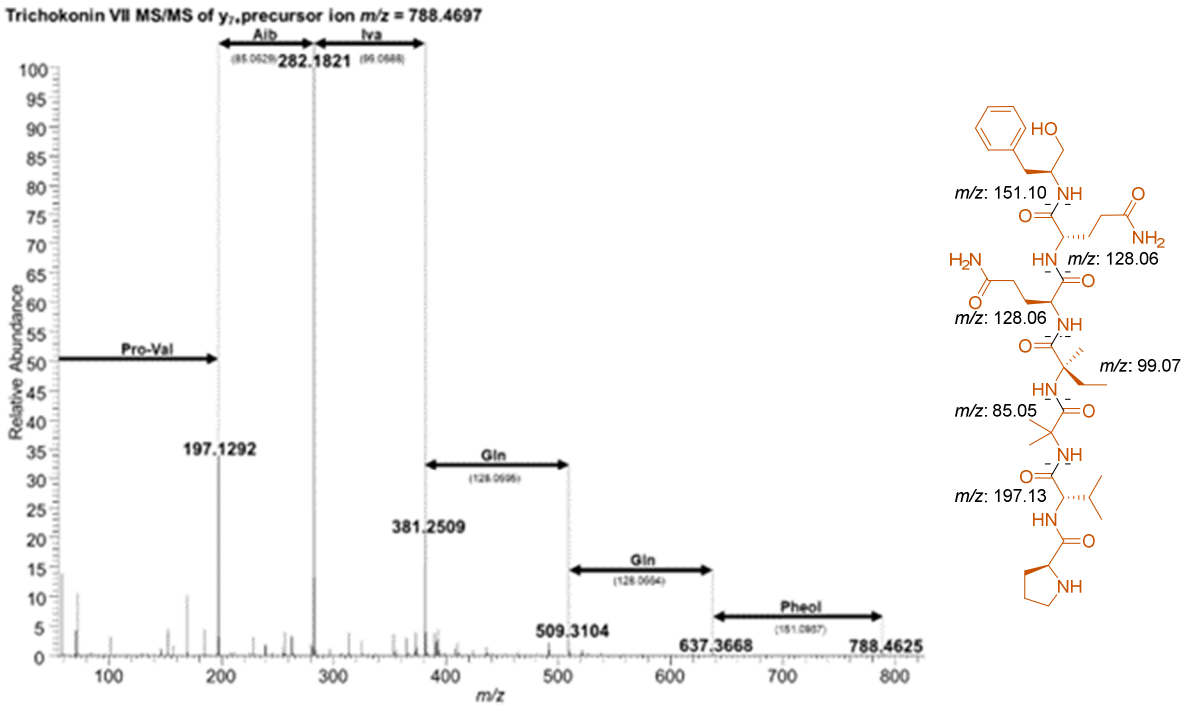

Notes. Fragmented amino acids are identified for the *y* positions of the peptaibol in the *m/z* range 55.0000-825.0000. Predicted fragmentation patterns and theoretical *m/z* values were generated in ChemDraw Professional v. 21.0.0.28. Data were collected on a Thermo Fisher Scientific Q-Exactive Plus Orbitrap mass spectrometer with positive mode electrospray ionization (ESI) coupled to a Waters Acquity UHPLC column (BEH C18, 1.7 µm, 2.1 × 50 mm, Waters Corporation, Milford, MA, USA). Fragmentation data were collected with a normalized collision energy of 30 eV for the high-energy collision-induced dissociation (HCD).

Fig. 1.11 Trichokonin VIII ($C_{91}H_{151}N_{23}O_{24}$) full MS analysis from sample MSX29608-01077-126-2.

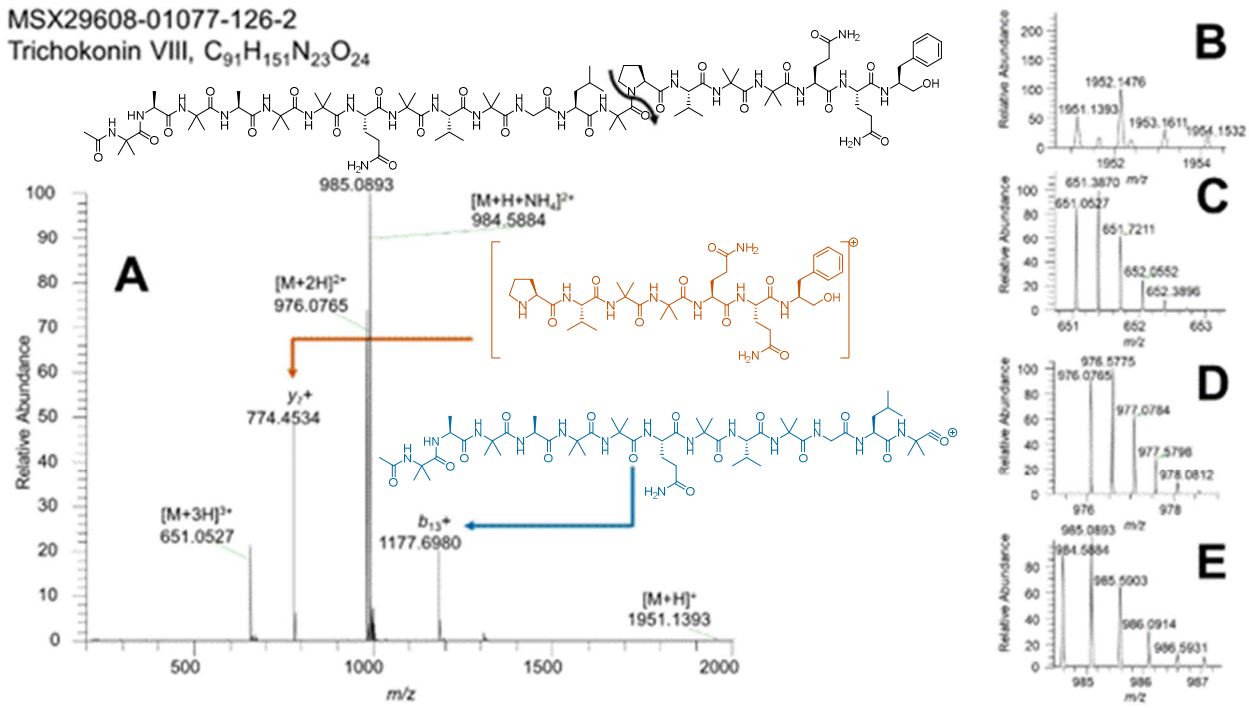

Notes. Panel A shows the full spectrum with diagnostic ions for Trichokonin VIII annotated. Primary in-source fragments y_7^+ and b_{13}^+ are highlighted with representative structures. Panels B-F show zoomed-in regions for each of the adducts labeled in panel A. Signature ions include *m/z* = 1951.1393 $[M + H]^+$, 1301.0947 $[2M + 3H]^{3+}$, 984.5884 $[M + H + NH_4]^{2+}$, 985.0893 (base peak) ^{13}C $[M + H + NH_4]^{2+}$, 976.0765 $[M + 2H]^{2+}$, 651.0527 $[M + 3H]^{3+}$, 774.4534 y_7^+, 1177.6980 b_{13}^+. Data were collected on a Thermo Fisher Scientific Q-Exactive Plus Orbitrap mass spectrometer with positive mode electrospray ionization (ESI) coupled to a Waters Acquity UHPLC column (BEH C18, 1.7 µm, 2.1 × 50 mm, Waters Corporation, Milford, MA, USA).

Fig. 1.12 Trichokonin VIII MS/MS from sample MSX29608-01077-126-2 of precursor ion *m/z* = 1301.7664 and b_{13+} precursor ion *m/z* = 1177.7003 at retention time t_R = 6.11 min.

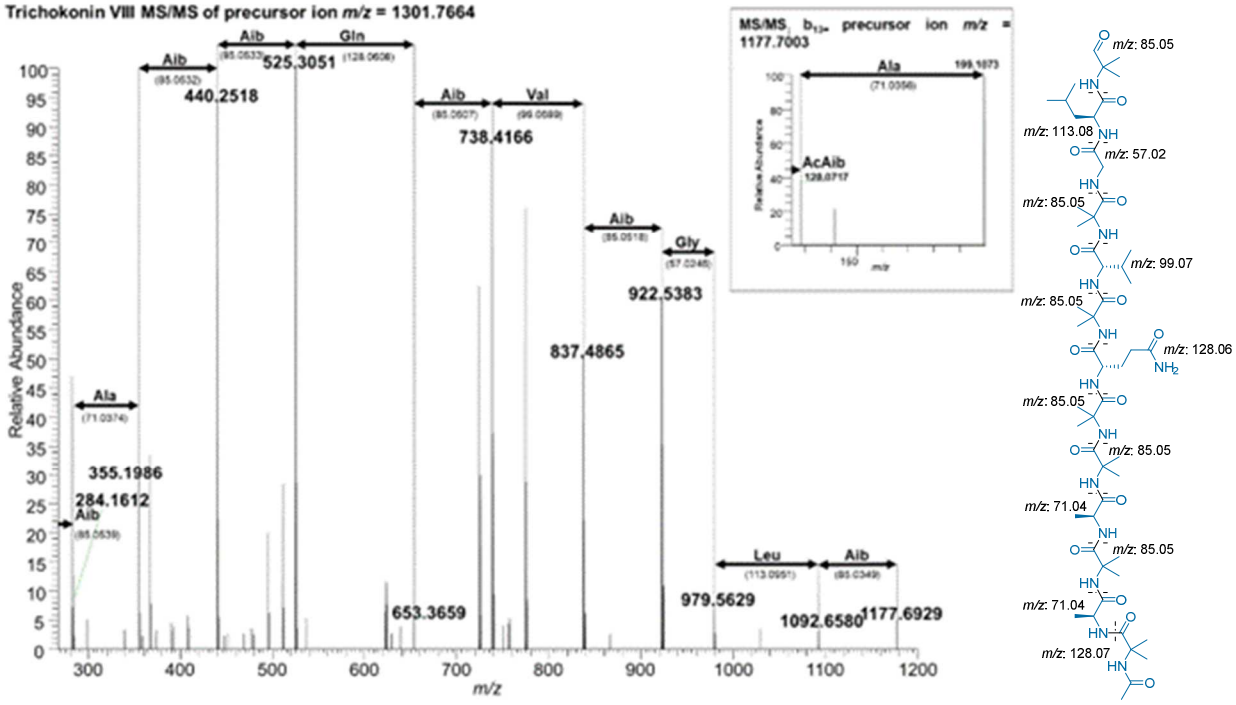

Notes. Fragmented amino acids are identified for the *b* positions of the peptaibol. The full sequence of Trichokonin VIII was determined matching literature as Ac-Aib[1]-L-Ala[2]-Aib[3]-L-Ala[4]-Aib[5]-L-Aib[6]-L-Gln[7]-Aib[8]-L-Val[9]-Aib[10]-Gly[11]-L-Leu[12]-Aib[13]-L-Pro[14]-L-Val[15]-Aib[16]-L-Aib[17]-L-Gln[18]-L-Gln[19]-L-Pheol[20]. Predicted fragmentation patterns and theoretical *m/z* values were generated in ChemDraw Professional v. 21.0.0.28. Data were collected on a Thermo Fisher Scientific Q-Exactive Plus Orbitrap mass spectrometer with positive mode electrospray ionization (ESI) coupled to a Waters Acquity UHPLC column (BEH C18, 1.7 µm, 2.1 × 50 mm, Waters Corporation, Milford, MA, USA). Fragmentation data were collected with a normalized collision energy of 30 eV for the high-energy collision-induced dissociation (HCD).

Fig. 1.13 Trichokonin VIII MS/MS from sample MSX29608-01077-126-2 of y^{7+} precursor ion *m/z* = 774.4548 at retention time t_R = 6.09 min.

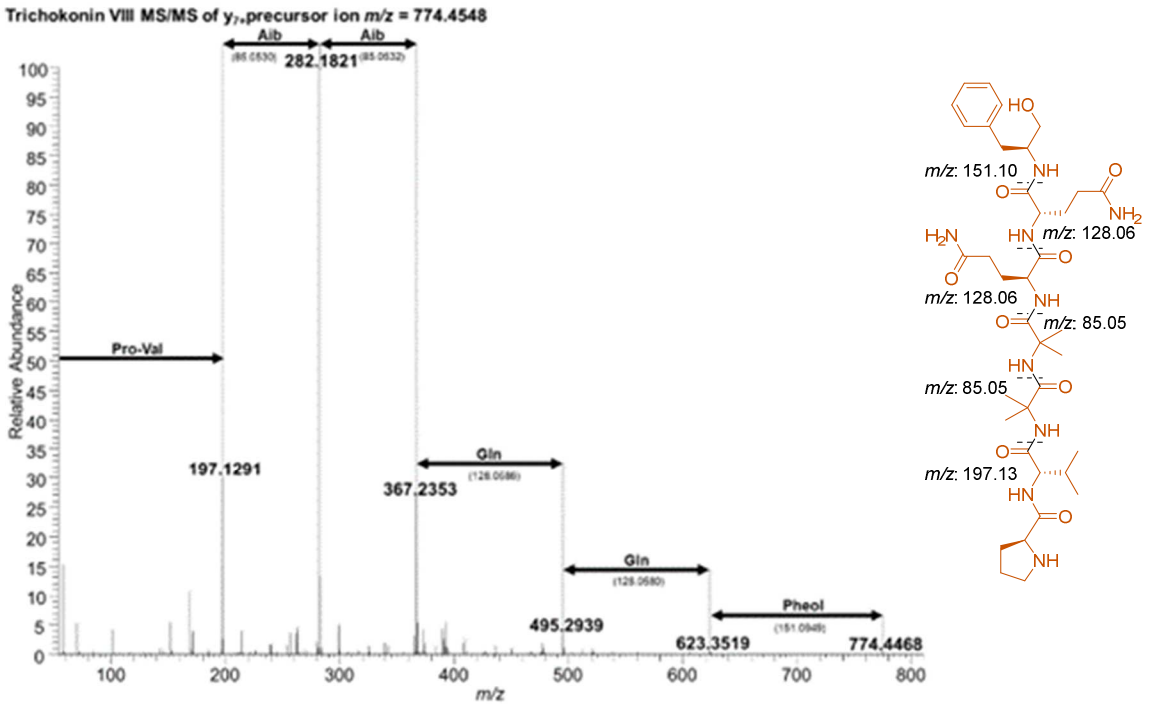

Notes. Fragmented amino acids are identified for the *y* positions of the peptaibol in the *m/z* range 54.0000-810.0000. Predicted fragmentation patterns and theoretical *m/z* values were generated in ChemDraw Professional v. 21.0.0.28. Data were collected on a Thermo Fisher Scientific Q-Exactive Plus Orbitrap mass spectrometer with positive mode electrospray ionization (ESI) coupled to a Waters Acquity UHPLC column (BEH C18, 1.7 µm, 2.1 × 50 mm, Waters Corporation, Milford, MA, USA). Fragmentation data of Trichokonin VIII were collected with a normalized collision energy of 30 eV for the high-energy collision-induced dissociation (HCD).

Table 1.2 Summary of MS/MS fragmentation data of Trichokonin VII and Trichokonin VIII isolated from extract of the fungus MSX29608.

b	Trichokonin VII	*	Trichokonin VIII	**	y	Trichokonin VII	*	Trichokonin VIII	**
b1	128.0711	128	128.0717	128	y2	197.1292	197	197.1291	197
b2	199.1089	199	199.1073	199	y3	282.1821	282	282.1821	282
b3	284.1611	284	284.1612	284	y4	381.2509	381	367.2353	367
b4	355.1981	355	355.1986	355	y5	509.3104	509	495.2939	495
b5	440.2517	440	440.2518	440	y6	637.3668	367	623.3519	623
b6	511.2898	511	525.3051	525	y7	788.4625	788	774.4468	774
b7	639.3470	639	653.3659	653					
b8	724.4013	724	738.4166	738					
b9	823.4705	823	837.4865	837					
b10	908.5220	908	922.5383	922					
b11	965.5483	965	979.5629	979					
b12	1078.6322	1078	1092.6580	1092					
b13	1163.6812	1163	1177.6929	1177					

Notes. MS^n of Trichokonin VII* and Trichokonin VIII** reported in literature (41, 42).

Fig. 1.14 ^{1}H NMR spectrum (500 MHz, top) and ^{13}C NMR spectrum (175 MHz, bottom) both in DMSO-d_6, of compound Trichokonin VII.

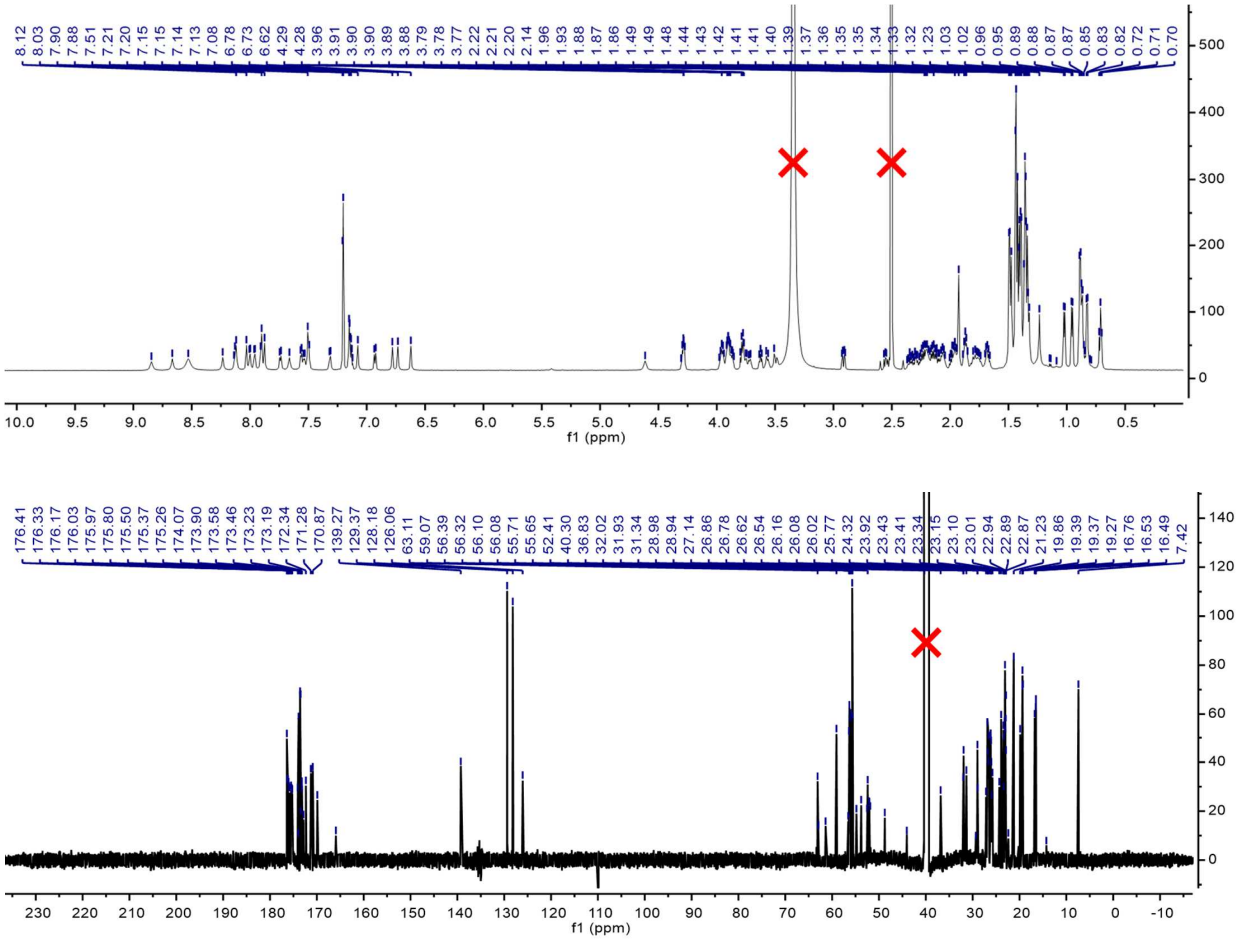

Fig. 1.15 ^{1}H NMR spectrum (500 MHz, top) and ^{13}C NMR spectrum (175 MHz, bottom) both in DMSO-d6, of compound Trichokonin VIII.

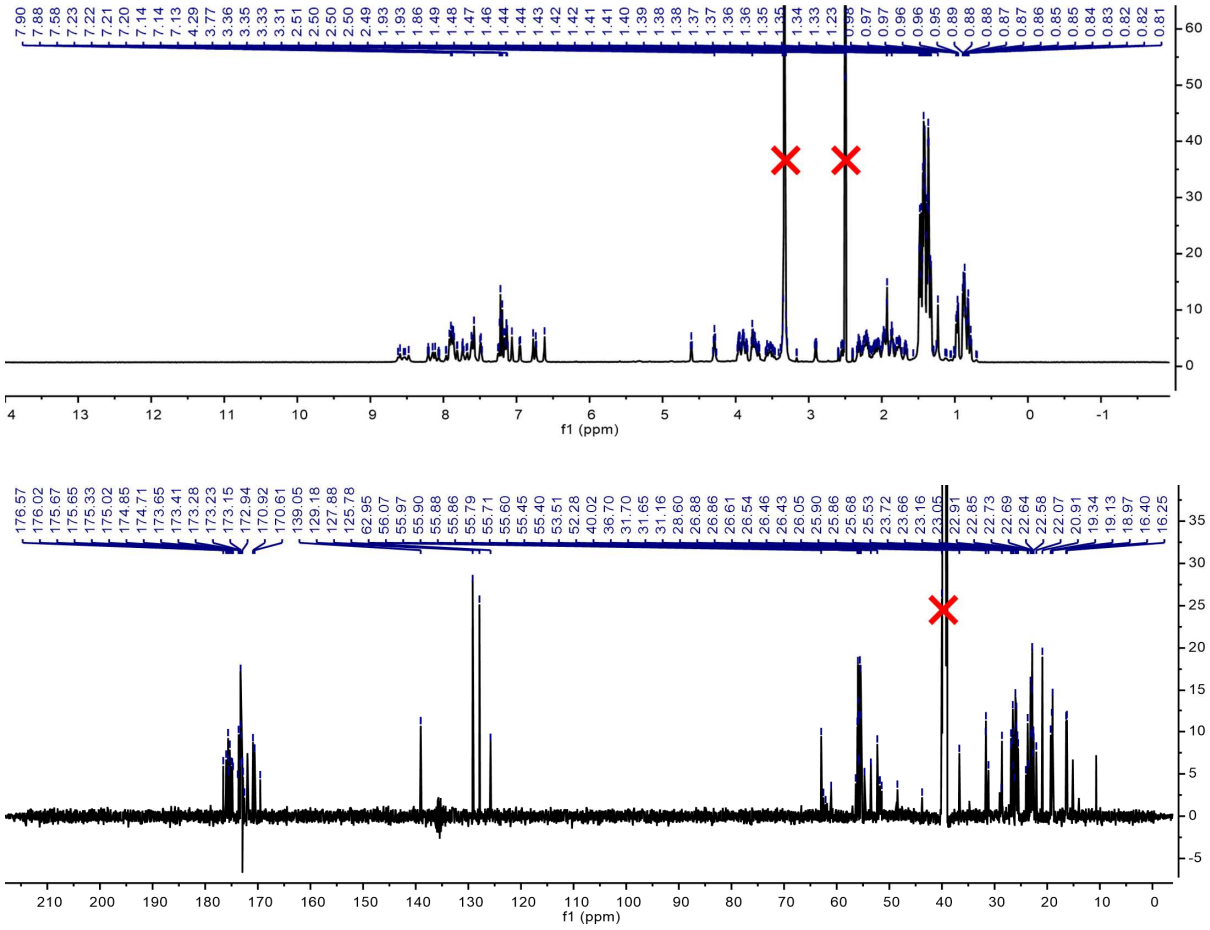

Determination of amino acid configuration for Trichokonin VII and Trichokonin VIII was conducted by Marfey's analysis (**Fig.** 1.16**, Fig.** 1.17**,** Table 1.**3**). The sequence of Trichokonin VII was determined as Ac-Aib^{1}-L-Ala^{2}-Aib^{3}-L-Ala^{4}-Aib^{5}-L-Ala^{6}-L-Gln^{7}-Aib^{8}-L-Val^{9}-Aib^{10}-Gly^{11}-L-Leu^{12}-Aib^{13}-L-Pro^{14}-L-Val^{15}-Aib^{16}-D-Iva^{17}-L-Gln^{18}-L-Gln^{19}-L-Pheol^{20}. The sequence of Trichokonin VIII was determined as Ac-Aib^{1}-L-Ala^{2}-Aib^{3}-L-Ala^{4}-Aib^{5}-L-Aib^{6}-L-Gln^{7}-Aib^{8}-L-Val^{9}-Aib^{10}-Gly^{11}-L-Leu^{12}-Aib^{13}-L-Pro^{14}-L-Val^{15}-Aib^{16}-L-Aib^{17}-L-Gln^{18}-L-Gln^{19}-L-Pheol^{20}. Positions *b6* and *b17* distinguish the sequences of Trichokonin VII and Trichokonin VIII from one another. These peptaibols were previously reported in literature and observed in several previous studies (11, 41-43).

Fig. 1.16 Conversion of L-glutamine and D-glutamine to L-glutamic acid and D-glutamic acid, respectively after Marfey's hydrolytic reaction.

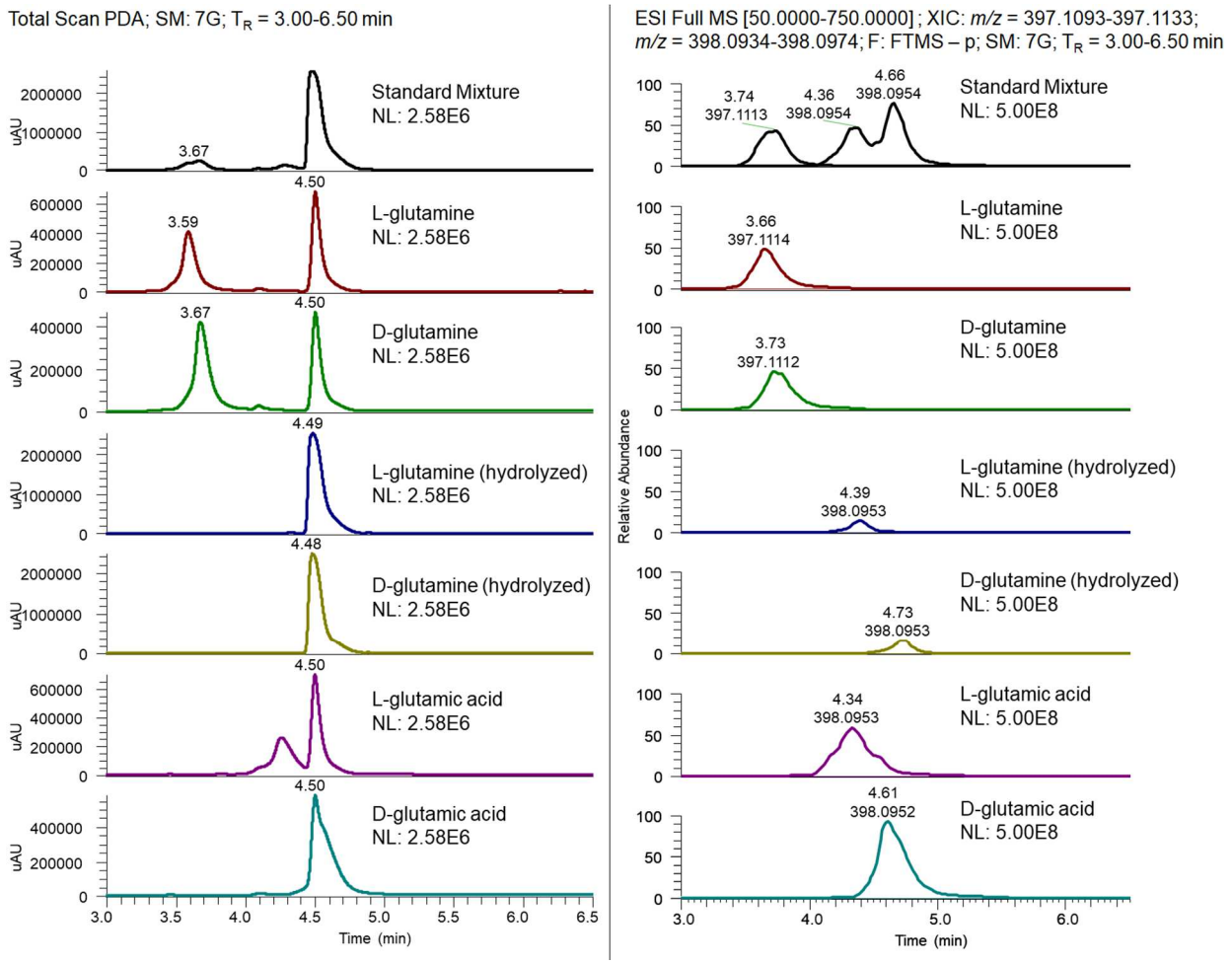

Notes. Total scan PDA data (left) demonstrates the absence of peaks for L- and D-glutamine (3.59 and 3.67 min respectively) after each standard was hydrolyzed. XIC negative mode MS data for the masses of glutamine reacted with Marfey's (calcd. *m/z* = 397.1111) and glutamic acid reacted with Marfey's (calcd. *m/z* = 398.0752) are shown (right). Accurate masses confirm the conversion of L- and D-glutamine to L- and D-glutamic acid respectively after hydrolysis. Data were collected on a Thermo Fisher Scientific Q-Exactive Plus Orbitrap mass spectrometer with negative mode electrospray ionization (ESI) coupled to a Waters Acquity UHPLC column (BEH C18, 1.7 µm, 2.1 × 50 mm, Waters Corporation, Milford, MA, USA).

Fig. 1.17 Determination of peptide configurations by Marfey's analysis of Trichokonin VII and Trichokonin VIII.

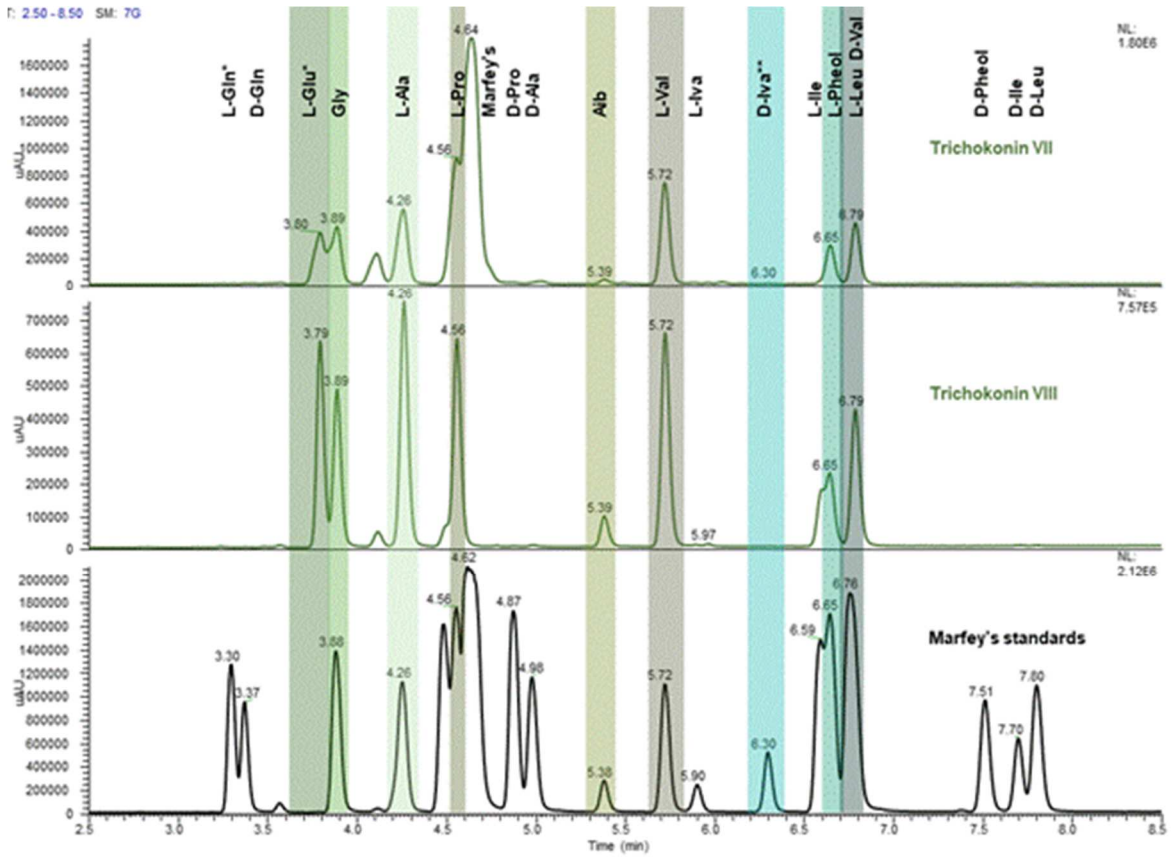

Notes. Total scan photodiode array (PDA) detection coupled to UHPLC chromatography data of Trichokonin VII and Trichokonin VIII with signals confirmed in comparison to L- and D-amino acid standards. Data were collected on a Thermo Fisher Scientific Q-Exactive Plus Orbitrap mass spectrometer with negative mode electrospray ionization (ESI) coupled to a Waters Acquity UHPLC column (BEH C18, 1.7 µm, 2.1 × 50 mm, Waters Corporation, Milford, MA, USA).

*L-glutamine was present as confirmed by accurate mass in **Fig.** 1.10 but converted to L-glutamic acid after hydrolysis prior to Marfey's reaction, confirmed in **Fig.** 1.16**, Fig.** 1.17**,** and Table 1.**3**. This phenomenon has been described previously (44).

**D-Iva was observed in lower abundance than other standards by MS analysis (2.52×10^7) and confirmed by accurate mass and MS retention time as compared to the standard (*m/z* = 368.1221, t_R = 6.37).

Table 1.3 Marfey's analysis summary of Trichokonin VII and Trichokonin VIII.

Amino Acid	(L)	(D)	Trichokonin VII	Trichokonin VIII
Gln	3.30	3.37	3.80*	3.79*
Gly	3.88		3.89	3.89
Ala	4.26	4.98	4.26	4.26
Pro	4.56	4.87	4.56	4.56
Aib	5.38		5.39	5.39
Val	5.72	6.76	5.72	5.72
Iva	5.90	6.30	6.30	-
Ile	6.60	7.70	-	-
Pheol	6.65	7.51	6.65	6.65
Leu	6.76	7.80	6.79	6.79

Notes. Comparison of PDA detection retention times for the L- and D- amino acid standards and compounds Trichokonin VII and Trichokonin VII after reaction in the Marfey's procedure. All assignments also confirmed by accurate mass and retention time.

*observed the conversion of L-Gln to L-Glu in Marfey's reaction and confirmed by accurate mass, see **Fig.** 1.16**-Fig.** 1.17**,** Table 1.**3)**.

Fungal Strains

MSX41370, the source of pyridoxatin, was identified as *Tolypocladium* sp., *Ophiocordycipitaceae, Hypocreales, Ascomycota* (**Fig.** 1.18). MSX29608, the source of Trichokonin VII and Trichokonin VIII, was identified as *Trichoderma deliquescens* (*=Hypocrea lutea*) (**Fig.** 1.19) (45-48).

Fig. 1.18 MSX41370 fungal identification.

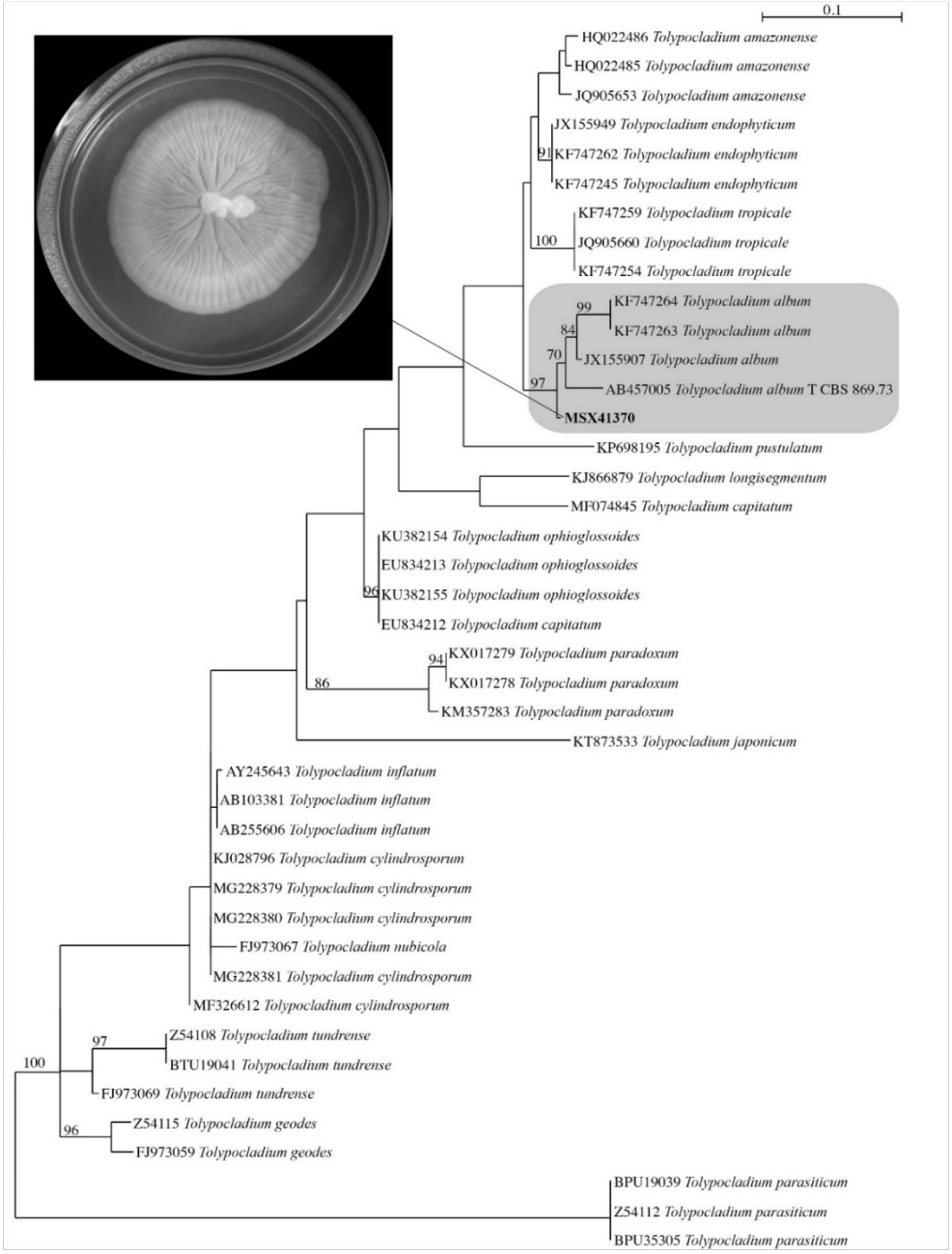

Notes. Phylogram of the most likely tree (–lnL = 3864.4 1341) from a PHYML analysis of 41 strains based on combined ITS nrDNA sequence data (481bp). Numbers refer to PHYML bootstrap support values ≥ 70% based on 1000 replicates. Strain MSX41370 is nested with the *Tolypocladium album* clade including the type strain CBS 869.73. Bar indicates nucleotide substitution per site. A 3–week–old culture of *Tolypocladium,* (MSX41370) on Difco, MEA media is shown.

Fig. 1.19 MSX29608 fungal identification.

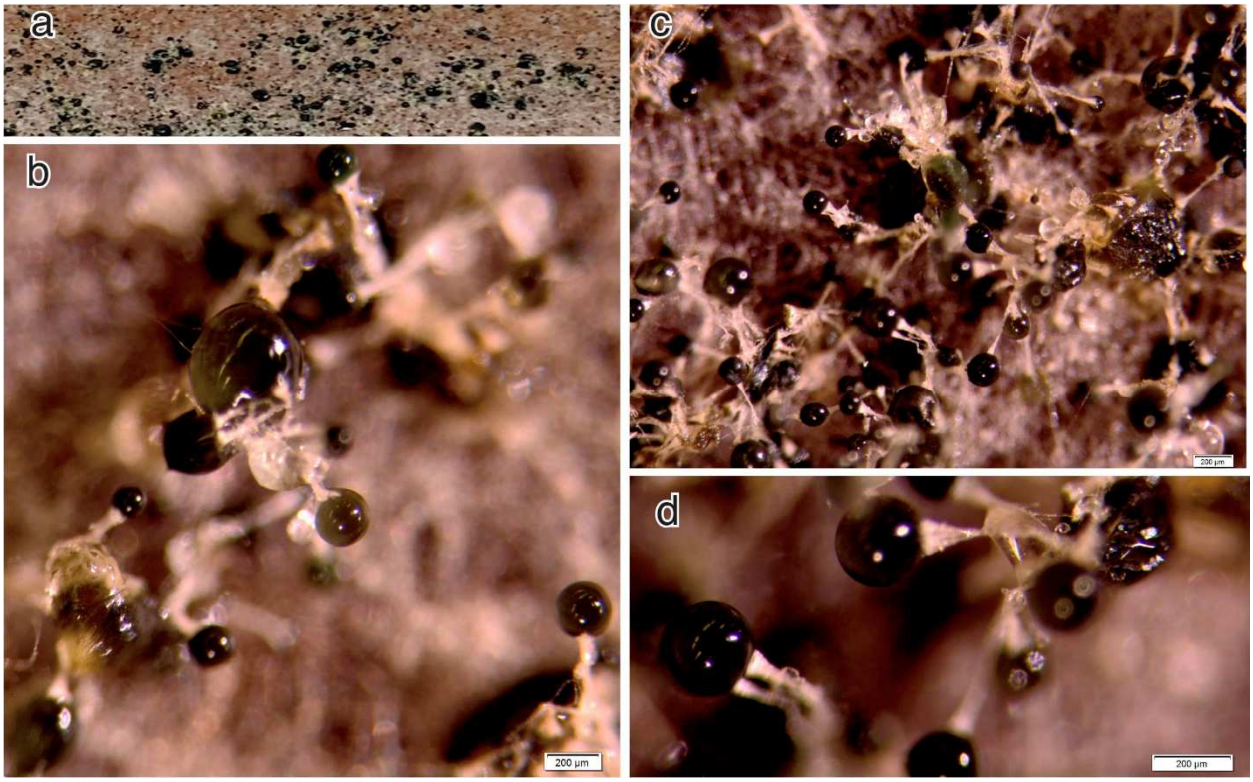

Notes. Morphological characteristics of *Trichoderma deliquescens* (MSX29608) A. Surface of fungal culture on potato dextrose agar; B-D. Conidiophores and conidial heads in culture, showing the conidia wrapped in a mucous exudate (46). Measure bars = 200 µm.

In vitro Antimicrobial Activity

Antimicrobial activity of pyridoxatin was evaluated in a broth microdilution assay against *A. baumannii* (AB5075), which demonstrated an MIC value of 38 µM, in comparison to the MIC of 27.7 µM for levofloxacin (Table 1.4). Pyridoxatin was tested against a panel of *A. baumannii* isolates: AB0057, ATCC 19606, ATCC BAA-1605, ATCC 17978 (8) and showed MIC values 38.0, 38.0, 19.0, 38.0, 38.0 µM respectively; levofloxacin MIC values 27.7, 27.7, 0.87, 27.7, 3.46 µM respectively (**Fig.** 1.20**, Table 1.4**) (49). Trichokonin VII and Trichokonin

VIII were also tested against *A. baumannii* (AB5075) with both demonstrating MIC values > 64.1 μM compared to the MIC of levofloxacin at 27.7 μM (**Fig.** 1.21**, Table 1.4**).

Table 1.4 Summary of fungal compound antimicrobial activities.

Isolate Name	Pyridoxatin	Trichokonin VII	Trichokonin VIII	Levofloxacin
A. baumannii AB5075	38.0	> 64.1	> 64.1	27.7
A. baumannii AB0057	38.0	-	-	27.7
A. baumannii ATCC 19606	38.0	-	-	0.87
A. baumannii ATCC BAA-1605	19.0	-	-	27.7
A. baumannii ATCC 17978	38.0	-	-	3.46

Notes. Summary of MIC (μM) antimicrobial activity of fungal compounds, pyridoxatin, Trichokonin VII and Trichokonin VIII against a panel of *A. baumannii* in comparison to known antimicrobial compound levofloxacin.

Fig. 1.20 Antimicrobial activity of pyridoxatin.

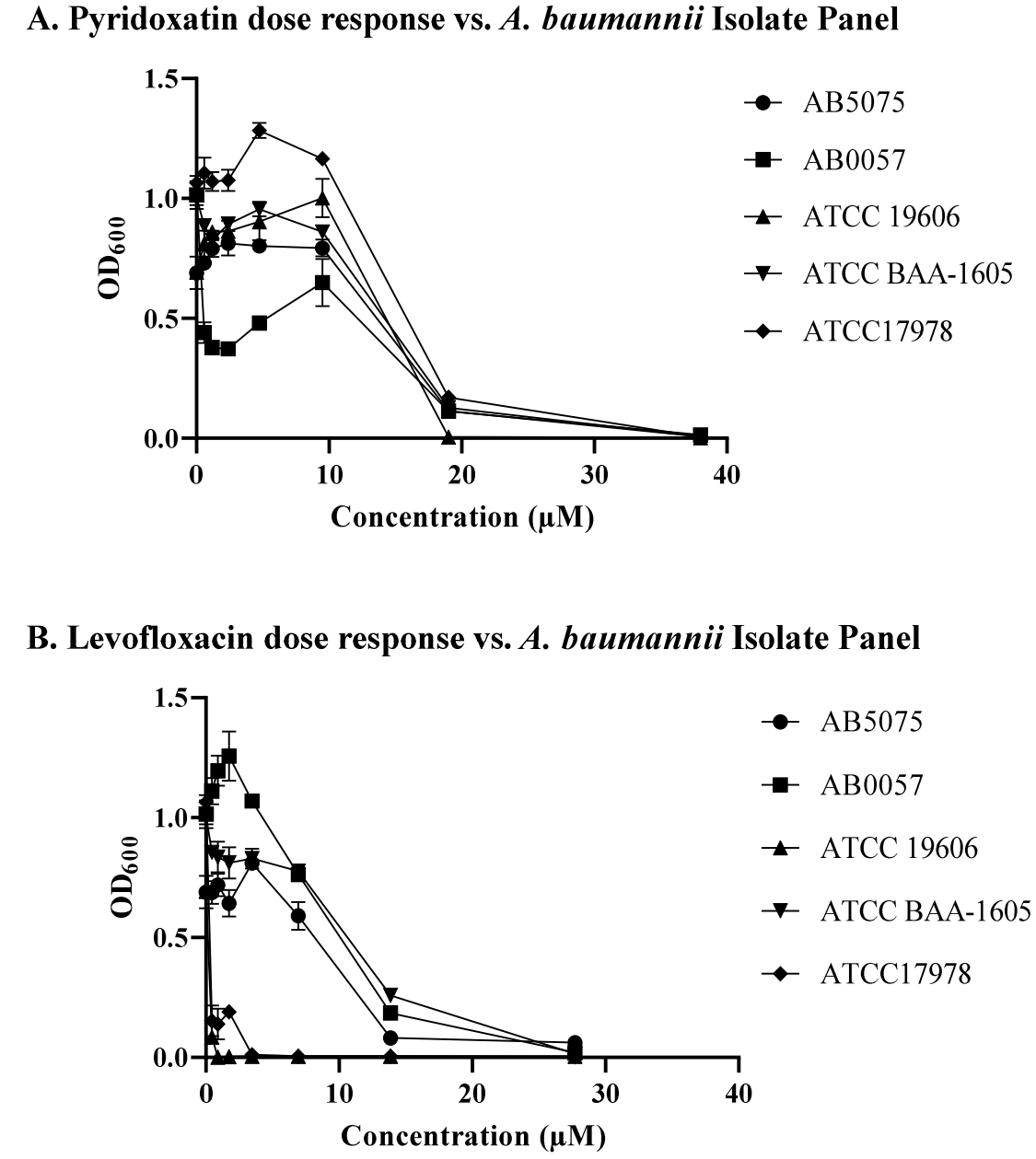

Notes. Antimicrobial assay of pure compounds in an eight point, two-fold dilution series against a panel of *A. baumannii* isolates, AB5075, AB0057, ATCC 19606, ATCC BAA-1605, ATCC 17978 (8). The range of concentrations for pyridoxatin, panel A, was 0 μM to 38.0 μM. The range of concentrations for clinical antibiotic levofloxacin, panel B, was 0 μM to 27.7 μM. The vehicle for all compounds was neat DMSO was diluted to 2% DMSO assay content. The 2%

DMSO vehicle did not inhibit bacterial growth. An average of triplicates was plotted, and error bars represent the standard error of the mean.

Fig. 1.21 Antimicrobial activities of Trichokonin VII and Trichokonin VIII.

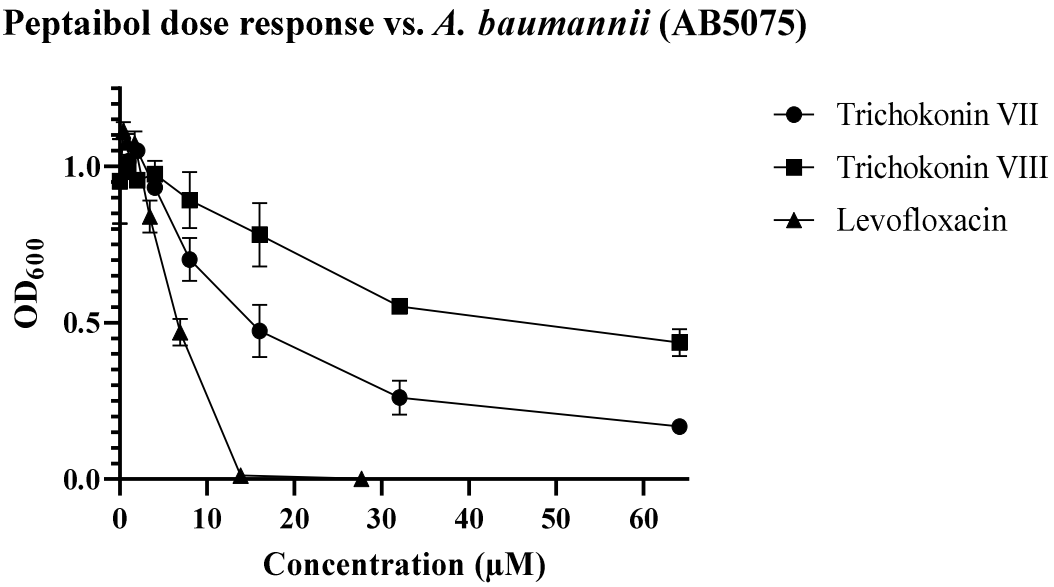

Notes. Antimicrobial assay of Trichokonin VII and Trichokonin VIII in an eight point, two-fold dilution series against a panel of *A. baumannii* isolates, AB5075, AB0057, ATCC 19606, ATCC BAA-1605, ATCC 17978. The range of concentrations for were 0 μM to 64.1 μM. The range of concentrations for the positive control, clinical antibiotic levofloxacin, were 0 μM to 27.7 μM. The vehicle for all compounds was neat DMSO was diluted to 2% DMSO assay content. The 2% DMSO vehicle did not inhibit bacterial growth. An average of triplicates was plotted, and error bars represent the standard error of the mean.

In vivo Toxicity and Efficacy

In an *in vivo Galleria mellonella* cytotoxicity model, pyridoxatin exhibited minimal toxicity at 150 mg/kg, with 90% survival after 5 days when injected alone (**Fig.** 1.22 **A).** The compound demonstrated antimicrobial efficacy *in vivo* against *A. baumannii* (AB5075), with 50% survival of infected *G. mellonella* after 5 days. Trichokonin VII and Trichokonin VIII were toxic to *G. mellonella* at a dosage of 150 mg/kg after 5 days, with 20% survival and 40% survival, respectively (**Fig.** 1.22 **B**). Trichokonin VII and Trichokonin VIII (both at dosages of

150 mg/kg) did not improve survival for *A. baumannii* infected *G. mellonella*. Dosage with both compounds resulted in only 10% survival after 5 days.

Fig. 1.22 *Galleria mellonella* screening of fungal compounds.

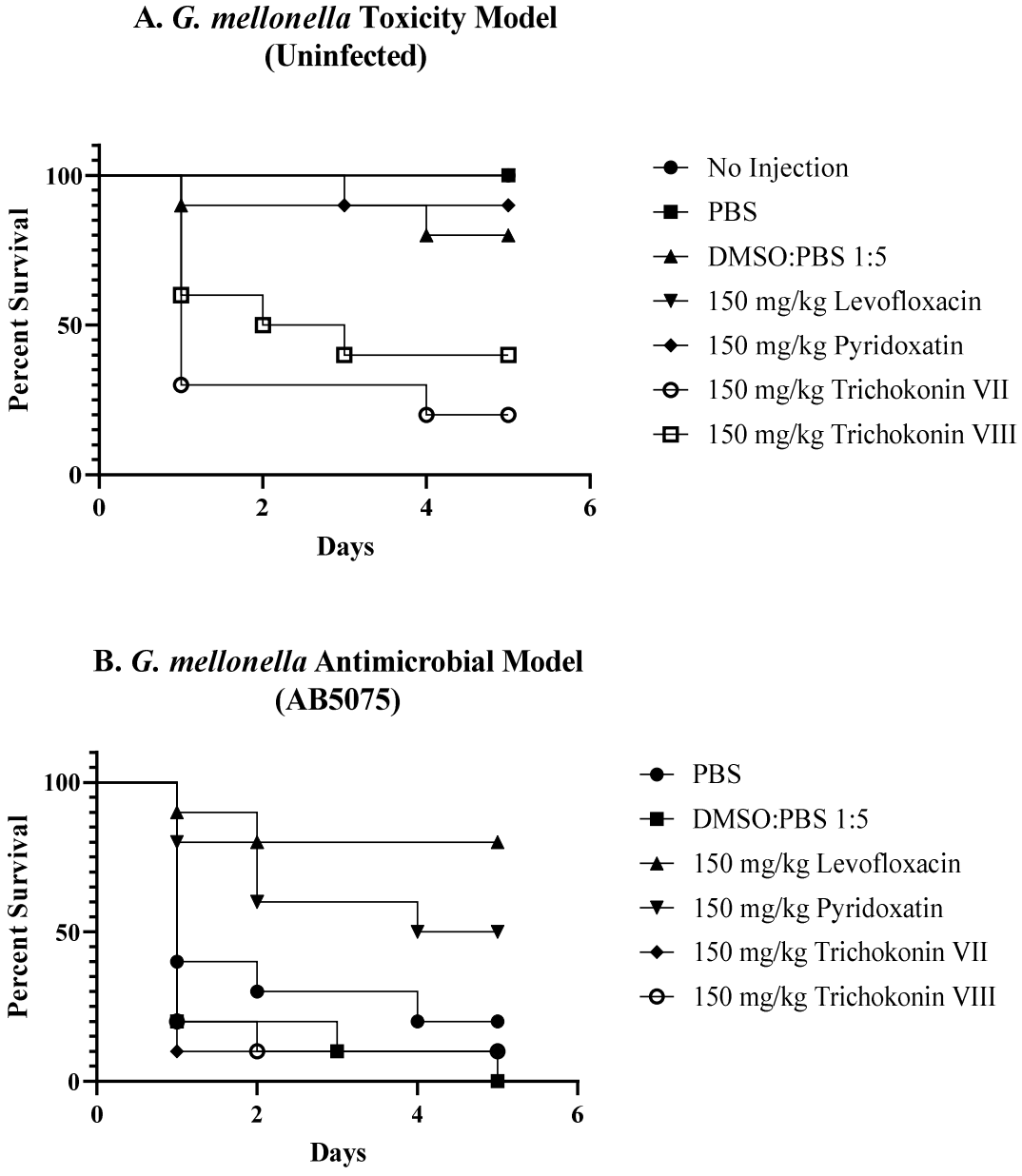

Notes. Uninfected *Galleria mellonella* antimicrobial compound toxicity experiment, shown in panel A. In vivo antimicrobial efficacy experiment against *G. mellonella* infected with *A. baumannii* (AB5075) at 5×10^6 CFU/mL, shown in panel B.

DISCUSSION

Screening of 2,500 extracts from the Mycosynthetix library followed by efforts to isolate and characterize active compounds yielded the primary lead pyridoxatin. This is the first report of the antimicrobial activity of pyridoxatin against *Acinetobacter baumannii.* Pyridoxatin was first discovered in 1991 by Yoshihiro Teshima and colleagues of the Institute of Applied Microbiology, University of Tokyo in the search for free radical scavenging and antimicrobial compounds from fungi (10). Antimicrobial activity had previously been reported for pyridoxatin in both Gram-positive methicillin-resistant *Staphylococcus aureus* and Gram-negative *Escherichia coli* (50-52). An *in vivo* model with *Caenorhabditis elegans* showed effectiveness of pyridoxatin as an antimicrobial agent, promoting survival at doses comparable to fluconazole. The compound has been reported as non-toxic when tested up to 121.6 μM in non-neoplastic, immortalized human prostatic epithelial (RWPE-1) cells and normal human bronchial epithelium (HBE) cells (52). A conclusive mechanism of action has not yet been determined for the antimicrobial activity of pyridoxatin, although speculation of a role in DNA synthesis inhibition has been proposed, with the hydroxamic acid moiety playing a key role in gelatinase A inhibition (39).

Trichokonin VII and Trichokonin VIII were previously identified in *Trichoderma* fungal extracts (41-43). These compounds fall under the class of peptaibols, which are fungal metabolites commonly produced by fungi of the species *Trichoderma* and composed of 5-20 amino acid residues, including α-aminoisobutyric acid (aib) and N-terminus amino alcohol residues (53). Peptaibols have high structural variability and broad biological applications, including antimicrobial activity due membrane disruption (43).

It is clear from these studies that Trichokonin VII and Trichokonin VIII are not promising leads for antimicrobial development, given their weak activity and high toxicity in the *G. mellonella* model (**Fig.** 1.22). However, pyridoxatin does show promise for future development. The compound (MIC 38.0 μM) is less potent than levofloxacin (MIC 27.7 μM) in both the *in vitro A. baumannii* (**Fig.** 1.20) and *in vivo G. mellonella* (**Fig.** 1.22) model, but its activity against a highly drug-resistant pathogen makes it a worthy candidate for lead optimization through synthetic or semi-synthetic approaches. Future studies to investigate mechanism of action and structure activity relationships would also be worthwhile. With an established total synthesis for pyridoxatin (40), such future studies may be feasible. Perhaps most importantly, pyridoxatin seems to be well tolerated in the *G. mellonella* model (**Fig.** 1.22). This finding bodes well for the potential clinical applicability of pyridoxatin, although further studies in other *in vivo* models are still needed.

MATERIALS AND METHODS

Rapid Qualitative Antimicrobial Assay

Initial rapid screening of the Mycosynthetix extract library was performed by adapting previously developed methods detailed in 1968 (an approach dating to the 1930's) to evaluate zones of antimicrobial inhibition with an agar diffusion technique (31, 54). All screening was performed with *A. baumannii* (AB5075). In preparation, an agar plate culture of *A. baumannii* (AB5075) was incubated for 12-16 hours at 37°C. The agar culture of *A. baumannii* was removed from incubator and stored at 4°C. An inoculum of *A. baumannii* was prepared by inoculating ~10 mL of Luria Bertani broth with 3-4 isolated colonies. The inoculum was incubated for 12-16 hours at 37°C, shaking at 200 rpm. 150 mL of agar was prepared from a

Luria Bertani broth recipe as follows: 25 g/L LB, 15 g/L agar, 100 mL nanopure water. Agar was autoclaved and a water bath was preheated to 50°C.

The agar solution was removed from the autoclave, and immediately placed in water bath but not allowed to solidify. Once agar was cool to touch but still molten, it was removed from water bath and transferred to the sterile hood. Inoculum (2.5 mL) was pipette transferred into the molten agar. Inoculated molten agar was returned to the water bath and mixed thoroughly without allowing bubbles to form. In the sterile hood, the inoculated molten agar was poured into sterile NUNC assay dishes (Sigma Aldrich, Corning® square bioassay dishes; CAS: CLS431272). The agar dishes were allowed to solidify (~30 min-1 hr). The extract, compound or control (5 μL) was pipetted directly on to the agar surface. A laminated template was placed beneath dish to guide sample placement and a map of sample placement was recorded. The agar dish was incubated 12-16 hours, at 37°C in incubator, then assessed for purity and consistency. Controls and extracts were assessed for antimicrobial activity and qualitative determination of inhibitory zones of bacterial growth where samples had diffused into the agar was recorded. Agar dishes were photographed on a clear dark surface.

Fungal Strain Identification

Strain MSX41370 was identified solely based on molecular data, since micromorphological analysis of the culture did not reveal any sporulation on potato dextrose agar (48). The entire internal transcribed spacer (ITS) region and the first 600 bp of the 5′ end of 28S large subunit (LSU) was PCR amplified and sequenced with primers ITS1F/ ITS4 or LROR and LR6 respectively using methods cited previously (48, 55-57). BLAST search using the ITS region in NCBI GenBank type database revealed that this strain had high similarities ≥97% with members of *Tolypocladium* (=*Elaphocordyeps*) in the *Ophiocordycipitaceae, Hypocreales,*

Ascomycota. Thus, maximum likelihood phylogenetic analysis was implemented in PHYML under the General Time Reversible evolutionary model using ITS and partial LSU data from recently published sequences in GenBank. Specifically, sequence data were downloaded from a study on *Tolypocladium cylindrosporum* and incorporated into a multiple alignment using MUSCLE (58, 59). All analysis were performed in SeaView v4.5.3 (60). Based on the PHYML maximum likelihood analysis, strain MSX41370 can be identified as *Tolypocladium album,* since MSX41370 grouped with other sequences of *T. album* and was sister to the type strain, CBS 869.73 with 97% bootstrap support (**Fig.** 1.18). However, due to the lack of morphological characters in culture; we conservatively refer to strain MSX41370 as a *Tolypocladium* sp., *Ophiocordycipitaceae, Hypocreales, Ascomycota*. Interestingly, pyridoxatin has been previously isolated from the genus *Tolypocladium* (39, 61). Importantly, recent mycological studies have proposed the use of the name *Tolypocladium* as priority over all other generic names, such as *Elaphocordyeps* and *Chaunopycnis*; therefore, these generic names should no longer be used in the literature (9). The sequence obtained in this study is deposited in GenBank (ITS and LSU: ON759752 (**Fig.** 1.18).

Dr. Barry Katz collected strain MSX29608 on 11 January 1987 from woody litter from a terrestrial habitat in Florida, USA. Identification of the fungal strain was performed using morphology and further confirmed by molecular sequence data (ITS region and *tef1*). The strain was grown on potato dextrose agar. Upon examination under the compound microscope, it was clearly evident that the fungus produced green conidia in large, dark green to black, deliquescent heads. After a review of the literature pertaining to *Trichoderma* taxonomy, based on the unique morphological characters (i.e., green conidia in dark green to black deliquescent heads) (Fig. 1.19), we were able to identify the strain as *Trichoderma deliquescens* (=*Hypocrea lutea*) (45-

47). In addition, we performed both PCR and bi-directionally Sanger sequencing of the ITS region (ITS1F and ITS4) as well as the translation elongation factor alpha (EF1-728F and TEF1LLErev) using methods outlined previously (45, 48, 62-65). BLAST search of the ITS region revealed a 100% match with *Trichoderma deliquescens* CBS 121131, type sequence (NR_134394.1; FJ860771). BLAST search with *tef1* region also showed a ≥97% match with *Trichoderma deliquescens* CBS 121131, type sequence (FJ860644) (45). As such, we identify strain MSX29608 as *Trichoderma deliquescens* (*Hypocreaceae, Hypocreales, Ascomycota*). The sequences obtained in this study were deposited in GenBank (ITS: ON759751; *tef1*: ON783801).

Fermentation, Extraction, and Isolation

A total of 2,500 fungal extracts from Mycosynthetix Inc (MSX) (Hillsborough, North Carolina) were tested for antimicrobial activity against highly drug-resistant *A. baumannii* (AB5075) (8). Extracts of strains MSX41370 and MSX29608 were ultimately prioritized. Pyridoxatin was identified in an extract of strain MSX41370, and since this compound could be purchased, isolation studies were not conducted.

To isolate the peptaibols (Trichokonin VII and Trichokonin VIII), strain MSX29608 was grown on rice following methods outlined previously (66). Extraction of this culture was performed by adding 60 mL of 1:1 CH_3OH-$CHCl_3$ to 250 mL Fernbach flasks (n=2). The samples were then chopped with a spatula and shaken overnight (~16 h and ~100 rpm) at room temperature. The samples were combined and celite was added before performing vacuum filtration. The remaining residues were washed with small volumes of MeOH. To the filtrate, 90 mL $CHCl_3$ and 150 mL H_2O were added. The biphasic solutions were stirred on a stir plate for 30 min. After separatory funnel transfer, the top aqueous layer was retained and the bottom organic layer was drawn off into a round-bottom flask, which was evaporated to dryness. The

dried organic extracts were pooled and resuspended in 100 mL of hexanes and 100 mL of 1:1 CH_3OH-CH_3CN. The biphasic solution was shaken vigorously and then transferred to a separatory funnel. The hexanes layer retained and the bottom CH_3OH-CH_3CN layer was drawn off into a round bottom flask and evaporated to dryness under vacuum (530 mg). This sample was separated by flash chromatography using a Teledyne ISCO Combiflash Rf with evaporative-light scattering detector (ELSD) and a photodiode array (PDA) detector, at 254 nm and 280 nm. A RediSep Rf Silica column (12 g) was used with a HPLC grade chloroform-hexane-methanol gradient at a flow rate of 30 mL/min. 32.0 column volumes were collected and resulted in 4 fractions. Fraction 4 (238.23 mg) was subjected to preparative RP-HPLC on a Varian ProStar HPLC Galaxie system using a Gemini C18 column with a gradient system of 50:50 to 60:40 CH_3CN:H_2O/0.1% formic acid over 20 min at a flow rate of 21.2 mL/min. Subfraction 7 (26.89 mg) yielded Trichokonin VII (retention time, t_R, = 15.25 min, 1.19 mg) and Trichokonin VIII (t_R = 17.90min, 1.93mg).

Pyridoxatin Identified in an extract of strain MSX41370. Isolation was not pursued. Full MS, MS/MS and retention times matched both literature reports and analysis of a purchased standard (Fig. 1.6) (36).

Trichokonin VII Isolated from an extract of strain MSX29608 as a white solid; UHPLC-MS $[M + H]^+$ *m/z* observed, 1951.1405. Calculated *m/z* of $[M + H]^+$, molecular formula $C_{91}H_{152}N_{23}O_{24}$, = 1951.1378 ($\Delta$ = 1.4 ppm). NMR data matched literature values (41).

Trichokonin VIII Isolated from an extract of strain MSX29608 as a white solid. UHPLC-MS $[M + H]^+$ *m/z* observed, 1951.1393. Calculated *m/z* of $[M + H]^+$, molecular formula $C_{91}H_{152}N_{23}O_{24,}$ = 1951.1378 (Δ = 0.8 ppm). NMR data matched literature values (41).

Ultra-high Performance Liquid Chromatography-Mass Spectrometry (UHPLC-MS)

Mass spectrometry data collection and analysis for the lead extracts to identify previously isolated compounds was carried out as detailed previously (36, 37). Mass spectrometry data collection for purified Trichokonin VII and Trichokonin VIII was performed on a Thermo Fisher Scientific Q-Exactive Plus Orbitrap mass spectrometer with electrospray ionization coupled to a Waters Acquity UHPLC column (BEH C18, 1.7 µm, 2.1 × 50 mm, Waters Corporation, Milford, MA, USA). Samples were prepared in Optima grade methanol at a concentration of 0.01 mg/mL. Data were collected in the full scan mode and data dependent tandem MS/MS mode, fragmenting precursor ions selected in a pre-determined inclusion list with a 2.0 *m/z* detection window. The Thermo Q-Exactive Plus mass spectrometer was operated in the positive mode with resolution of 70,000, full scan range of 200-2,000 *m/z*, maximum IT 100 ms, profile spectrum, and normalized collision energy of 30 eV for the high-energy collision-induced dissociation (HCD). Instrument conditions were as follows: spray voltage 3200 V, spray current 21.97 uA, capillary temperature 256.25°C, sheath gas 47.50, auxiliary gas 11.25, spare gas 2.25, probe heater temperature 350°C, and S-Lens RF level 50.00.

Column temperature was 40°C and sample temperature was 10°C. UHPLC analysis with a 3 µL injection volume was performed with a 0.3 mL/min flow rate with a binary solvent system including solvent A, water with 0.1% formic acid added, and solvent B, acetonitrile with 0.1% formic acid added. Gradient elution over a total of 10 minutes was performed, where conditions began at 85 % A : 15% B with these starting conditions held for one minute, then to 0 % A : 100 % B over 7 minutes with a 1.5 minute hold, returning to starting conditions for 0.1 minutes and held for 0.4 minutes. Data were analyzed with Thermo Xcalibur.

Marfey's Analysis

Marfey's analysis reactions and mass spectrometry methods were performed to confirm Trichokonin VII and Trichokonin VIII as described previously and matched reported literature (67). Chromatography conditions were modified from previous methods (68) to optimize distinct elution of amino acid standards and began with a solvent system of 95% A : 5% B, held for 0.5 min, to 85% A : 15% B for 0.5 min, reaching 55% A : 45% B over 7 min, then to 0% A : 100% B over 0.1 min with a 0.9 min hold before returning to starting conditions for 1 min. Further chromatography optimization with isocratic separation was required for amino acids standards containing L- and D-glutamine, where chromatography conditions began with a solvent system of 95% A : 5% B, held for 0.5 min, to 85% A : 15% B over 0.5 min with a 6 min isocratic hold, then reaching 50% A : 50% B over 1 min, then to 0% A : 100% B over 0.1 min with a 0.9 min hold before returning to starting conditions over 0.1 min and held for 0.9 min.

Nuclear Magnetic Resonance (NMR)

NMR spectral analyses were conducted in DMSO-d_6 for purified compounds Trichokonin VII and Trichokonin VIII on a JEOL ECA-500 NMR spectrometer operating at 500 MHz for 1D ^{1}H NMR experiments (JEOL Ltd.) or an Agilent 700 NMR spectrometer (Agilent Technologies) operating at 175 MHz for ^{13}C NMR. Residual solvent signals of DMSO-d_6 (δH = 2.50 and δC = 39.51) were used for referencing spectra and a tetramethylsilane (TMS) internal reference. MestReNova was used to integrate spectral data.

In vitro Antimicrobial Evaluation

Extracts, fractions and pure compounds were tested for inhibitory activity against highly drug-resistant *A. baumannii*, strain AB5075 using Clinical Laboratory Standards Institute (CLSI) guidelines (8, 35). A panel of *A. baumannii* isolates, AB0057, ATCC 19606, ATCC BAA-1605, and ATCC 17978 (8), were prepared in the same conditions as *A. baumannii* (AB5075). In brief,

to prepare the bacterial culture, a swab of cryopreserved stock of *A. baumannii* was T-streaked and incubated upon Luria-Bertani (LB) agar at 37°C in a humid environment for 16 h. A single colony was inoculated into 5 mL of Luria-Bertani broth and incubated at 37°C, shaking at 250 rpm for 16 h. A seed culture was started two hours prior to addition to 96-well microplate by diluting the inoculum into a total volume of 15 mL of LB broth (8). The OD_{600} value of this culture was measured with a Synergy H1 microplate reader (Biotek, Winooski, VT, USA) and the culture was adjusted to 5×10^5 colony forming units (CFU)/mL. Each well was uniformly inoculated with this standardized bacterial culture and co-incubated with vehicle control of 2% DMSO, positive control levofloxacin at 10 μg/mL (Sigma-Aldrich), or test compounds in 2% DMSO. Test compounds were prepared in an 8-point 2-fold dilution series ranging from 0 to 10 μg/mL and added to the 96-well microplate in triplicate, as well as duplicated in a control plate with no bacterial organism inoculation used for subtraction of any absorbance readings resulting from extracts and compounds. The minimum inhibitory concentration (MIC) was evaluated by quantitative and qualitative examination of wells in which no turbidity was observed. Inhibitory concentration at half-maximal growth (IC_{50}) was calculated using nonlinear regression analysis of the inhibitory dose-response curve from OD_{600} readings, stock concentrations and error (manually calculated as standard error of the mean) in GraphPad Prism version 9.3.1 software.

In vivo Toxicity and Efficacy Evaluation Against Galleria mellonella

Cytotoxicity of fungal compounds was measured in a modified *in vivo* model of *Galleria mellonella* (greater wax moth larvae) (12, 13). An inoculum of *A. baumannii* (AB5075) was incubated overnight in Luria-Bertani broth, shaking at 250 rpm, 37°C. A 1:3 dilution of the bacterial inoculum to LB broth served as a seed culture and was incubated under identical conditions for 2 h prior to bacterial injections of larvae. Larvae were injected in the first left

proleg with 10 µL of sterile phosphate buffered saline (PBS) to serve as a physical trauma control, 10 µL of 1:5 DMSO:sterile PBS to serve as a vehicle control, 10 µL of pure compound in 1:5 DMSO:sterile PBS (to ensure compound solubility) or 10 µL of levofloxacin in at 150 mg/kg 1:5 DMSO:sterile PBS as a positive control. Approximately two hours after the first injection, the seed culture of bacteria was pelleted in a centrifuge at 4,000 rpm for 10 min. The supernatant was discarded and the pellet was washed with 1 mL sterile PBS 3 times, then resuspended in 10 mL of sterile PBS. The optical density at 600nm was measured against a PBS blank diluted to 5×10^6 CFU/larvae. The second injection was in the last left proleg and performed with either 10 µL sterile PBS to serve as a physical trauma control of two injections, or 10 µL of *A. baumannii* (AB5075) suspended in sterile PBS at 5×10^6 CFU/larvae (12). After injections of treatments and bacterial inoculum were completed, all larvae were incubated at room temperature in petri dishes wrapped in aluminum foil to create a dark environment. Viability was evaluated every 24 h for 5 days and determined by response or lack of response to physical stimuli.

CHAPTER II: ANTIMICROBIAL BOTANICAL MECHANISMS OF ACTION: A *HYPERICUM CALYCINUM* CASE STUDY

INTRODUCTION

The use of botanicals as an integral part of medical practices dates back millennia and spans across cultures, such as Ayurvedic medicine originating in India and Traditional Chinese Medicine in Asia (69). Complementary or alternative health practices remain highly prevalent today, with 34% of adults in the U.S. using such health practices orthogonally to modern medical treatments based on data collected in 2012 (70). One major important aspect of complementary and alternative medicine is plant based dietary supplements, herein referred to as botanical natural products. Botanical natural products serve as a significant source of inspiration for modern medicine, with an estimated 25% of drugs prescribed worldwide originating from botanical sources (14, 71-73). Despite the popularity of botanical medicines, these treatments are often based upon oral traditions that have been translated into structure-function claims, but are unregulated by the FDA and often remain to be verified by scientific research for medicinal functions beyond nutritional value (74). While botanical medicines hold immense value to modern medical practices, rigorous scientific investigation is needed to verify if and how they are effective. Knowledge of active constituents and mechanisms of action of botanical natural products can aid in optimizing formulations to provide insight into effective approaches for their use in integrative medicine practices.

Developing new tools to validate and elucidate the mechanisms of botanical treatments already being administered in a largely unregulated manner can assist in validation of health effects and promoting awareness of potential underlying mechanisms. Traditional health practices based upon botanical natural products often incorporate similar species of plants for remedies, leading

to hypotheses that such redundancy may represent genuine, often uncharacterized activity (69). Studying these commonly utilized botanical species can serve as an important basis for application of knowledge gained from historical uses of botanical therapies. Turning to nature as sources of compounds with unique mechanisms of action and chemical scaffolds difficult to design or re-create synthetically broadens our structural diversity and potential health applications (75-77). Further, evaluation of complex botanical mixtures can help our understanding of chemical interactions that may occur only at the whole extract level, but not occur in isolation (14).

Several approaches have recently been developed for elucidation of a mechanism of action of small molecules such as those found in botanical medicines. These include bacterial cytological profiling, and genetic profiling such as the L1000 platform to decipher target and mechanism (5, 78, 79). Limitations to the current methods are observed when applied complex botanical extracts, as these techniques often rely upon studying a pure compound or a simplified mixture of compounds, relying upon prior knowledge of the active compound's identity and in the case of extract-derived natural products, requiring isolation and structural determination (80). The goal of the studies described herein was to design a predictive tool to characterize mechanism of action for complex botanical extracts. Towards this goal, we sought to employ mass spectrometry-metabolomics to simultaneously provide insight into biological activity and reveal correlations between mechanism of action with chemical composition**.** In these studies, we used the botanical species, *Hypericum calycinum* L. (Hypericaceae). This plant also known as creeping St. John's wort, Aaron's beard, or *Pyin-nyar-lin-kar* in Myanmar traditional medicine, is a summer, dawn-blooming ornamental botanical related to the medicinal plant, *Hypericum perforatum* L. (St. John's wort) (81-83). Recent studies have reported antimicrobial activity of *H. calycinum* and its known constituents against various Gram-positive pathogenic bacteria, including *Staphylococcus aureus*,

Streptococcus sp., *Corynebacterium diphtheriae*, and *Bacillus subtilis* (16, 84). Here, we sought to demonstrate the applicability of new approaches for identifying active extract constituents and predicting their mechanism of action using the antimicrobial activity of *H. calycinum* extracts against methicillin-resistant *Staphylococcus aureus* (MRSA) as a model system. We employed a clinically relevant MRSA strain (USA300 LAC AH1263), which is susceptible to some botanical compounds as a representative bacterial strain that demonstrates antimicrobial resistance (15). Six antibiotics were selected as positive controls based upon their clinical use in the treatment of MRSA infections. These antibiotics act via three different mechanisms of action: tetracycline and tigecycline (30S ribosomal subunit); moxifloxacin and levofloxacin (DNA gyrase); teicoplanin and vancomycin (cell wall disruption, peptidoglycan component MurNac pentapeptide) (85).

The chemical composition of *H. calycinum* has been well characterized in several studies, notably producing phloroglucinols, flavonoids and xanthones (81, 84, 86-89). *H. calycinum* has also been extensively studied for its biosynthetic pathways, including that of its ability to produce the polyprenylated acylphloroglucinol (PPAP) metabolite hyperforin and metabolites possessing a xanthone scaffold (90-97). Hyperforin in particular is a known antimicrobial compound (previously reported to have activity against MRSA) and widely produced by *Hypericum* sp. including *H. calycinum* (98). In comparison to other species in the genus, *H. calycinum* is notably distinct in its lack of the naphthodianthrone, hypericin, a photosensitizer abundant in *H. perforatum* (82, 99). Because the antimicrobial properties and chemical constituents of *H. calycinum* have been well characterized, this botanical serves as an ideal candidate for developing predictive tools for characterizing antimicrobial mechanisms of action in complex botanical mixtures.

RESULTS AND DISCUSSION

Antimicrobial Activity in vitro

Evaluation of *H. calycinum* extract, its four derived fractions (**Fig. 2.1**) (tested at 1, 10 and 100 µg/mL), and a standard of hyperforin (tested at 0.1, 1 and 10 µg/mL) against MRSA revealed antimicrobial activity in the extract, fraction 1, fraction 3 and hyperforin as compared to a vehicle control and clinically relevant antibiotic vancomycin (**Fig. 2.2**).

Fig. 2.1 Workflow of *H. calycinum* extraction and fractionation.

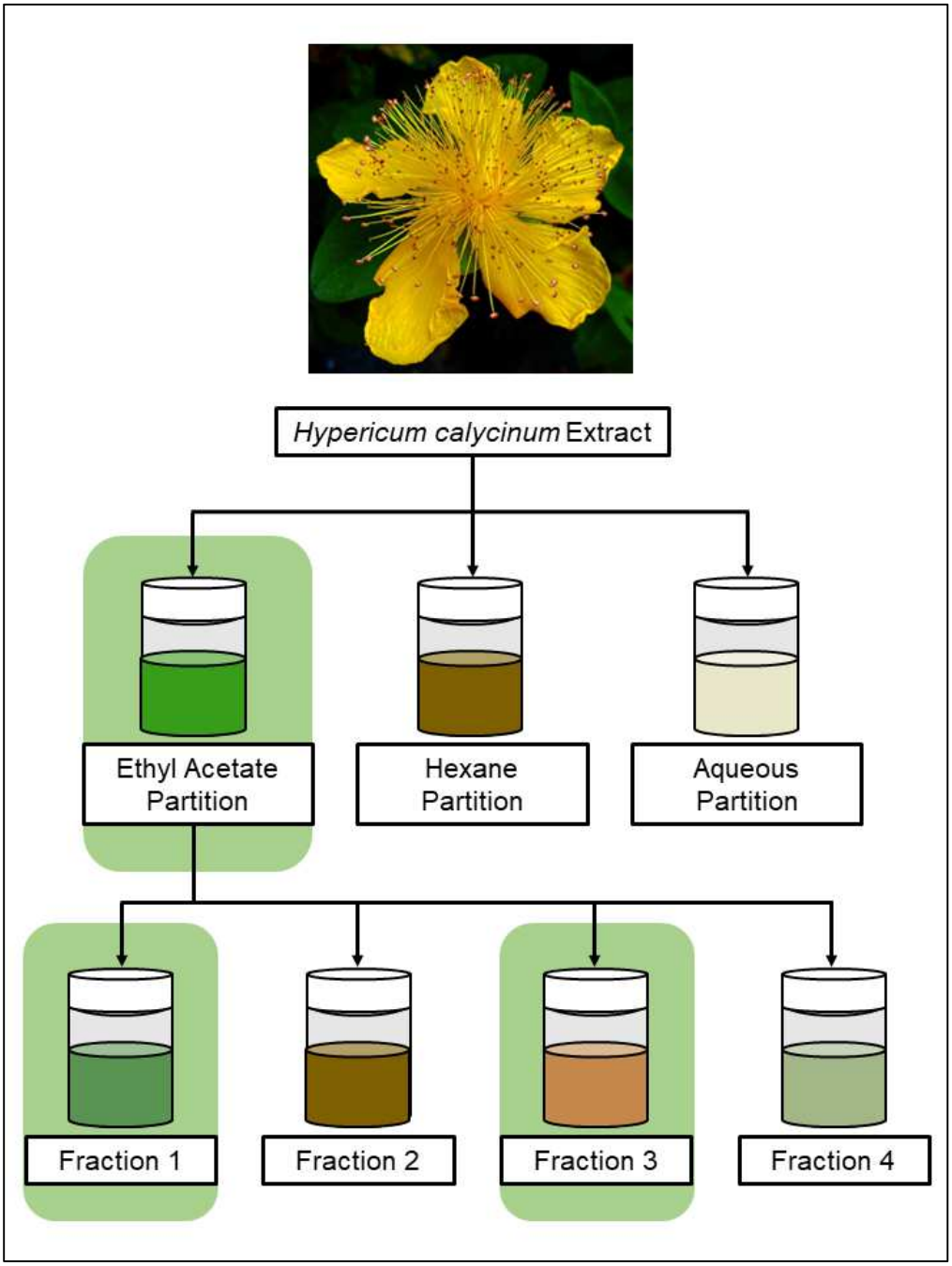

Notes. Green boxes indicate samples with antimicrobial activity against MRSA (USA300 LAC AH1263).

Fig. 2.2 Antimicrobial activity of *H. calycinum* extracts, fractions 1-4 and known compounds vs. MRSA.

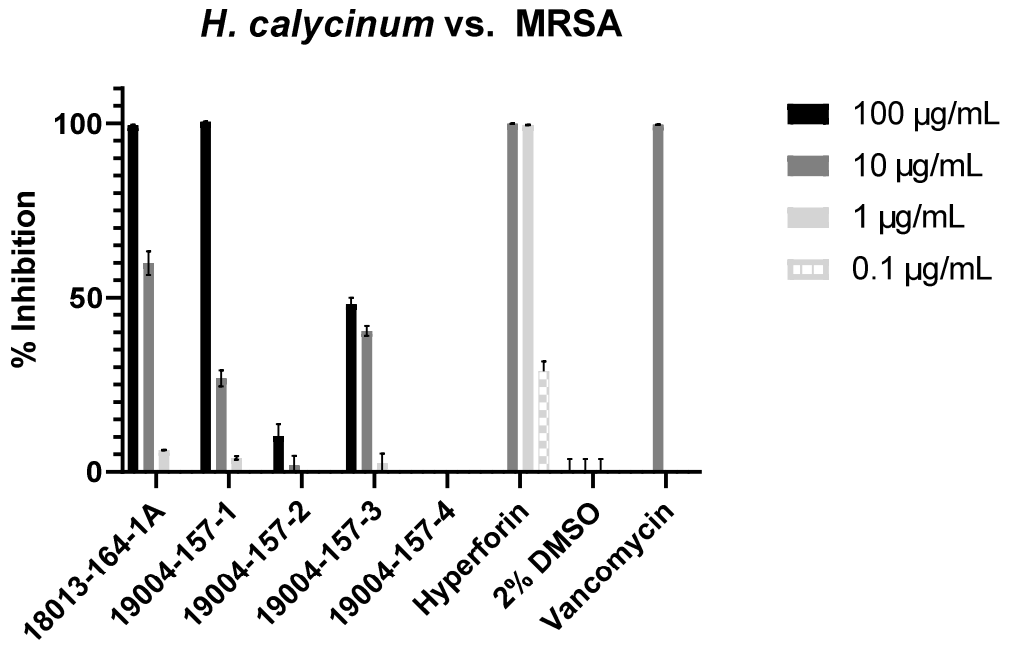

Notes. Tested in ten-fold dilutions between 0.1-100 µg/mL vs. MRSA (USA300 LAC AH1263).All samples tested in comparison to positive control, vancomycin, at 10 µg/mL. The vehicle for all compounds was neat DMSO was diluted to 2% DMSO assay content. The 2% DMSO vehicle did not inhibit bacterial growth. An average of triplicates was plotted, and error bars represent the standard error of the mean. Inhibitory % was calculated in Excel as ((average OD_{600} of vehicle control – OD_{600} of one biological replicate) / average OD_{600} of vehicle control) * 100.

Antimicrobial Annotation Model of H. calycinum Extracts and Fractions against MRSA

Applying metabolomics methods previously developed (17-19, 22, 100, 101), *H. calycinum* derived extract and fractions were evaluated by incorporation of antimicrobial bioactivity data as % inhibition (values derived from **Fig. 2.2**) with the triplicate sample injection chemical feature data set and analyses by Partial-Least Squares (PLS) regression scores and loadings plots (**Fig. 2.3**) and a selectivity ratio (SR) plot (**Fig. 2.4**). Triplicate samples clustered

together appropriately in the scores plot (**Fig. 2.3 A**), and multiple features were identified by the loadings plot (**Fig. 2.3 B**) as contributing to the variation amongst samples. The SR plot, predicting similar and additional features associated with antimicrobial activity shown in Error! eference source not found. was used to guide subsequent putative annotations.

Fig. 2.3 Antimicrobial annotation model metabolomics PLS scores (A) and loadings (B) of *H. calycinum* extract and fractions 1-4 vs. MRSA.

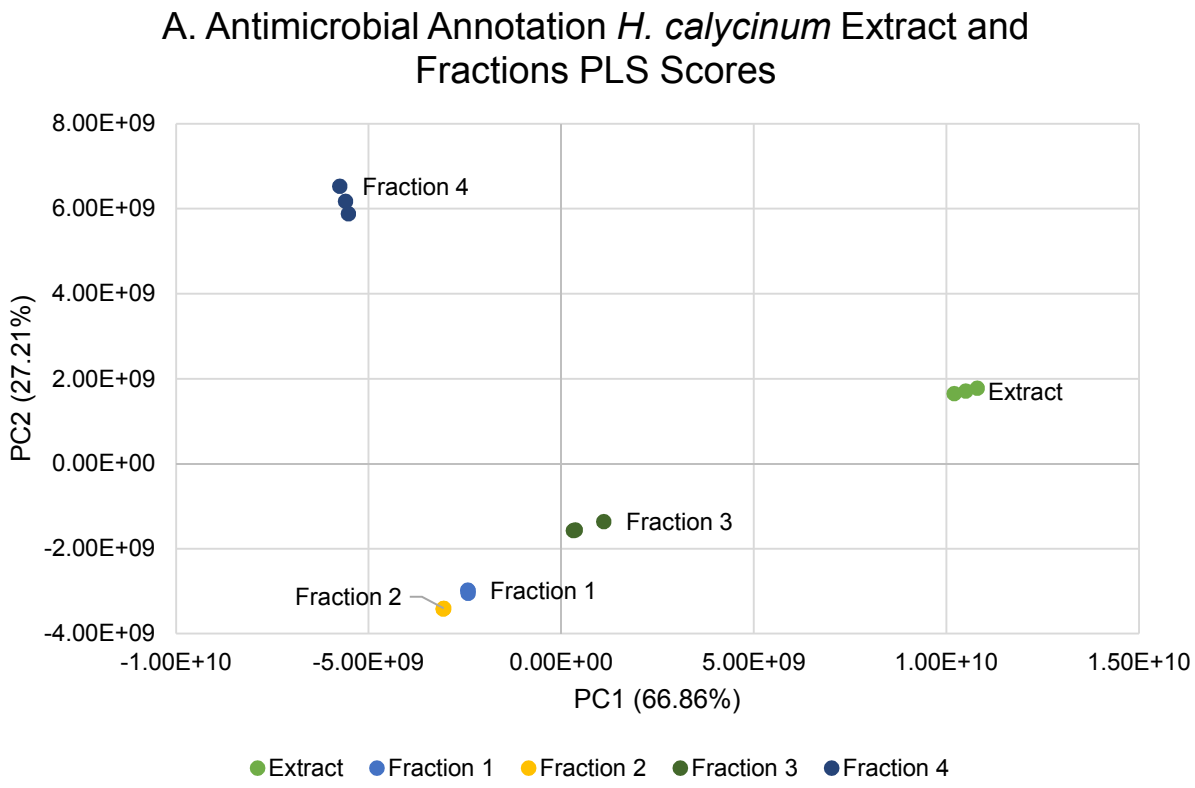

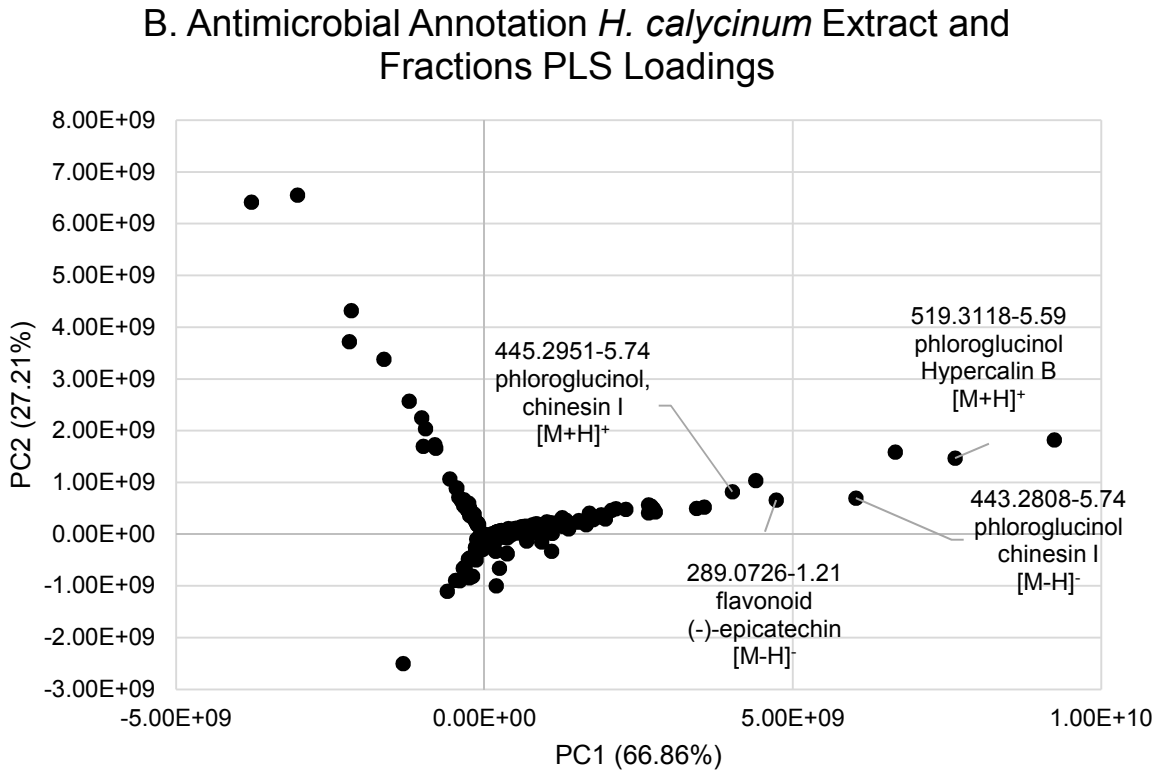

Notes. Tentative annotation of *m/z*-t_R features based upon accurate mass and previously reported literature observance in *Hypericum* sp., as compared to the Dictionary of Natural Products 31.1 database. Putative assignments include features as follow (structures shown in **Fig. 2.5**) chinesin I (1) at 445.2951-5.74 $[M+H]^+$ and 443.2808-5.74 $[M-H]^-$, hypercalin B (2) at 519.3118-5.59 $[M+H]^+$, and (-)-epicatechin (3) at 289.0726-1.21 $[M-H]^-$.

Fig. 2.4 Antimicrobial Annotation model metabolomics PLS selectivity ratio (SR) of *H. calycinum* vs. MRSA.

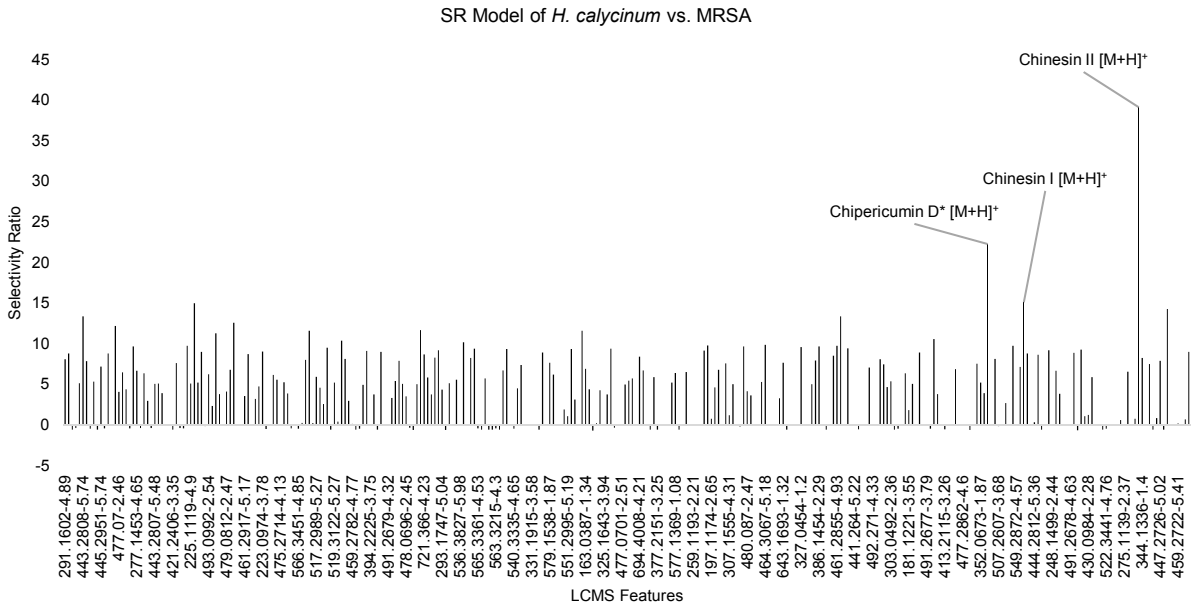

Notes. Antimicrobial annotation model PLS selectivity ratio (SR) plot incorporating mass spectrometry *m/z*-t_R pair features and biological antimicrobial % growth inhibition data of *H. calycinum* extract and fractions 1-4 vs. MRSA (USA300 LAC AH1263). Tentative annotation of *m/z*-t_R features is based upon accurate mass and previously reported literature observance in *Hypericum* sp., as compared to the Dictionary of Natural Products 31.1 database. Putative assignments of features (structures shown in **Fig. 2.5**) include chinesin I (1) at 445.2877-5.74 $[M+H]^+$, chinesin II (4) at 431.2796-5.32 $[M+H]^+$ and chipericumin D (5) at 461.29-4.6 $[M+H]^+$.

*Putative annotation matches multiple previously reported compounds.

Antimicrobial Annotation

Putative assignments of features from **Fig. 2.3-Fig. 2.4** have their structures and a summary of antimicrobial activity reports shown in **Fig. 2.5**. Tentative annotation levels, defined in previous studies (102), were identified by accurate mass and previous literature reports as present in *Hypericum* sp. (Level 3) or specifically *in H. calycinum* (Level 3a). The related phloroglucinols chinesin I (**1**), Level 3a, and chinesin II (**4**), Level 3a, were previously observed

in *H. calycinum* and chinesin I has reported antimicrobial activity against *S. aureus* with an MIC 3.13 µg/mL (81, 103). The phloroglucinol hypercalin B (**2**), Level 3a, observed in *H. calycinum* has been previously reported as antimicrobial against *S. aureus* with an MIC_{50} of 0.5 µg/mL (104, 105). The flavonoid (-)-epicatechin (**3**), Level 3a, was previously observed in *H. calycinum* and has been reported as inactive against *S. aureus* though has previously been observed to synergistically potentiate antimicrobial activity of other compounds by destabilizing the cell wall (88, 106, 107). Phloroglucinol chipericumin D (**5**), Level 3, was previously observed in *H. chinense* and has no reported antimicrobial activity **(108)**. The expected compound hyperforin (**6**), known to be present in *H. calycinum* and an antimicrobial against *S. aureus* with a reported MIC of 1.0 µg/mL (88, 98), was not predicted by the SR plot nor observed in the mass spectral data of the *H. calycinum* extract or fractions, though destructive degradation of hyperforin has been previously reported (109-111). Follow up experiments must be performed to quantify detection limits of hyperforin or its degradation products in the *H. calycinum* extract and fractions.

Fig. 2.5 Tentatively annotated structures 1-6 previously identified in *Hypericum* sp. (81, 108, 112-115).

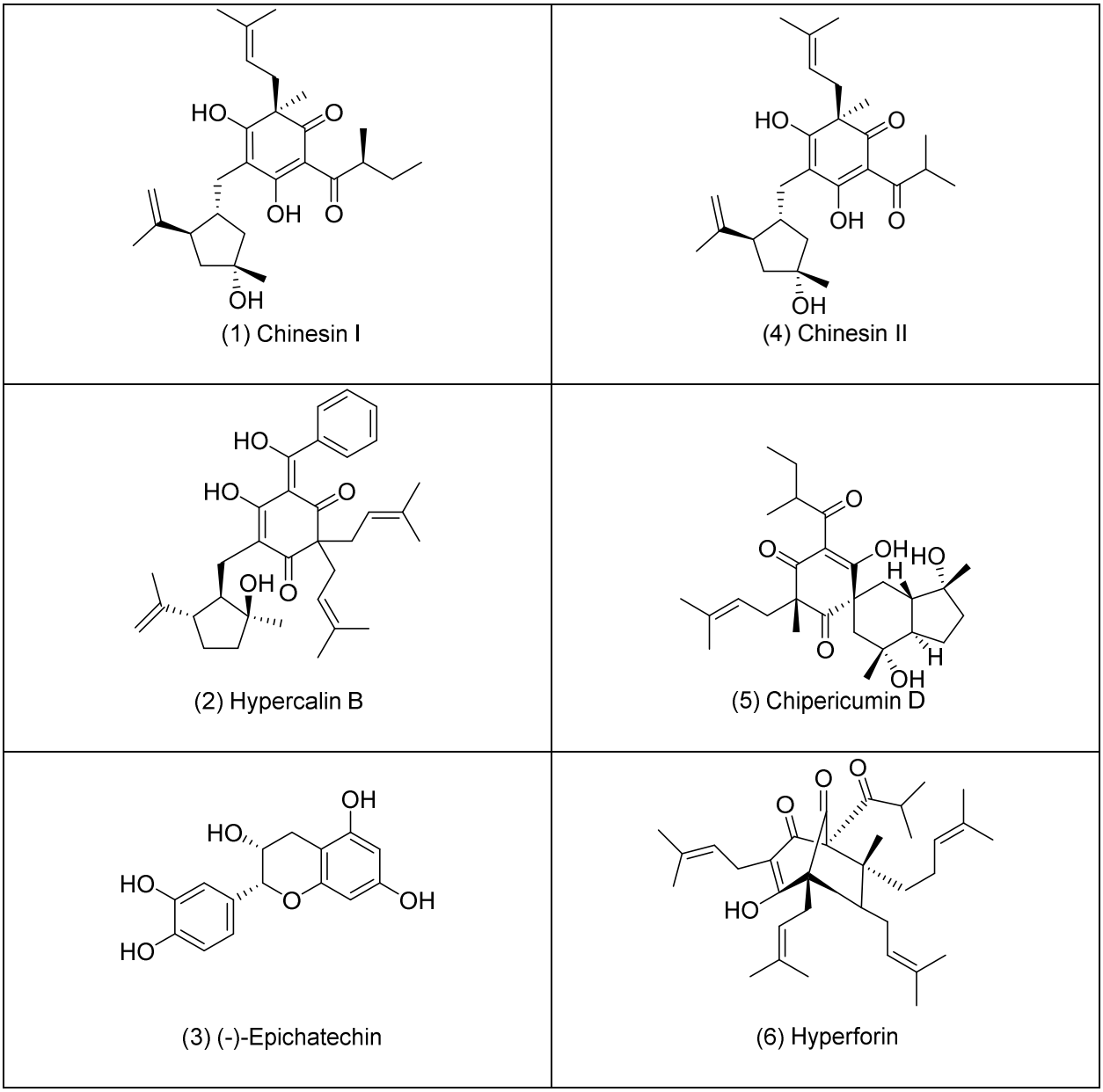

Mechanism of Action Model

Metabolomics methods were applied to the mass spectrometry mechanism of action data set evaluating extracellular matrices of MRSA exposed to sublethal concentrations of botanical or antibiotic (**Fig. 2.6)**. Prioritization of the samples by antimicrobial activity (guided by **Fig.**

2.2) determined inclusion criteria for the mechanism of action studies, in which 8-point, 2-fold dilution MICs were tested at concentration ranges appropriate to each sample to obtain a sub-lethal datapoint for each treatment (**Fig. 2.6)**. With principal component analysis (PCA) and plotting features exclusively found in both antibiotics belonging the same mechanism of action class, clustering by mechanism of action was observed with vancomycin with teicoplanin (cell wall disruption), moxifloxacin with levofloxacin (DNA gyrase) and tetracycline with tigecycline (30S ribosomal subunit) (**Fig. 2.7**). The *H. calycinum* extract, active fraction and acylphloroglucinol hyperforin standard were each compared in this manner to the antibiotics to predict their mechanism of action.

Fig. 2.6 Antimicrobial dose response of clinical antibiotics and *H. calycinum* extract, fraction 1 and pure compounds vs. MRSA.

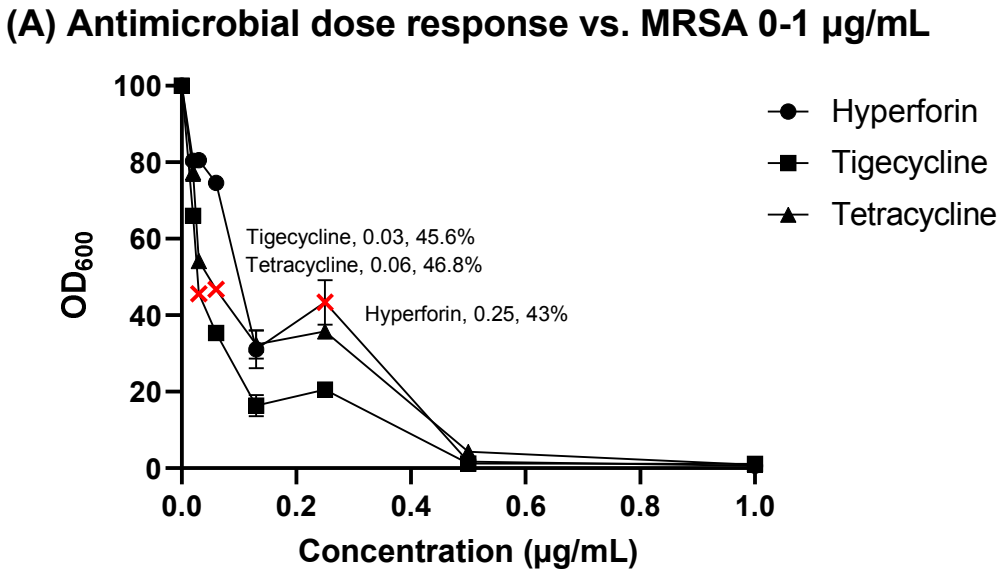

(B) Antimicrobial dose response vs. MRSA 0-10 µg/mL

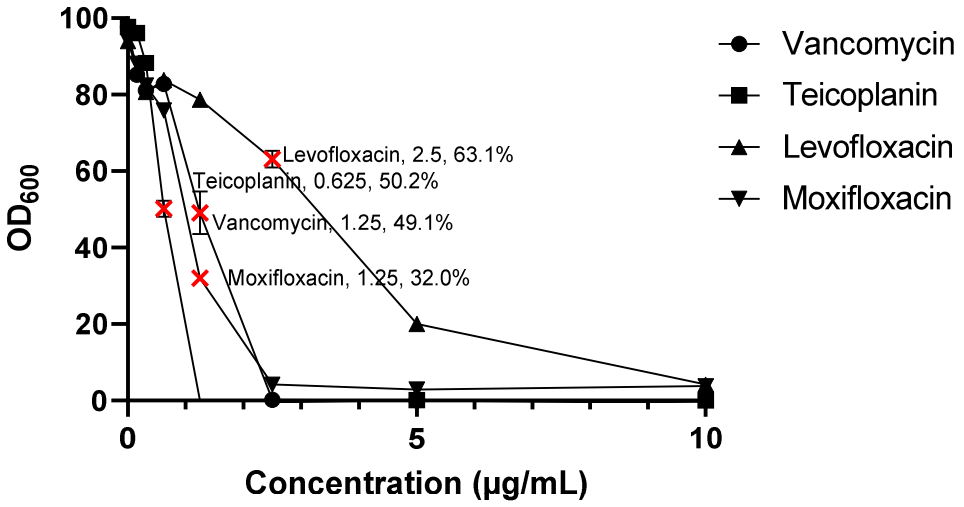

(C) Antimicrobial dose response vs. MRSA 0-100 µg/mL

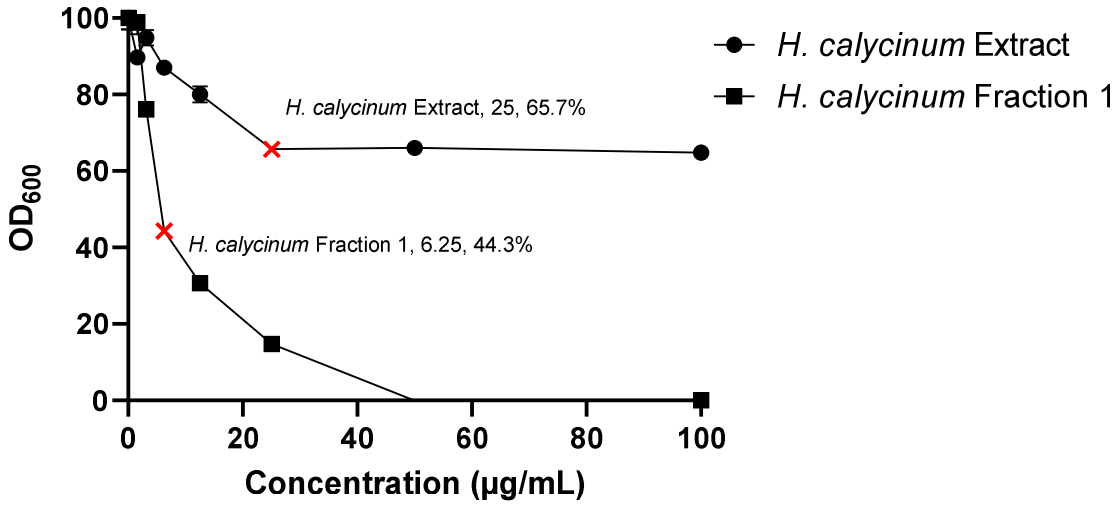

Notes. Antimicrobial dose response vs. MRSA (USA300 LAC AH1263). Antimicrobial assay of six clinically relevant antibiotics, botanical *H. calycinum* extracts, fractions and botanical pure compounds in an eight point, two-fold dilution series. The range of concentrations was 0-1 µg/mL (A), 0-10 µg/mL (B), and 0-100 µg/mL (C). The vehicle for all compounds was neat DMSO was diluted to 2% DMSO assay content. The 2% DMSO vehicle did not inhibit bacterial growth. An average of triplicates was plotted, and error bars represent the standard error of the mean.

Fig. 2.7 Mechanism of action prediction model PCA scores (A) and loadings (B).

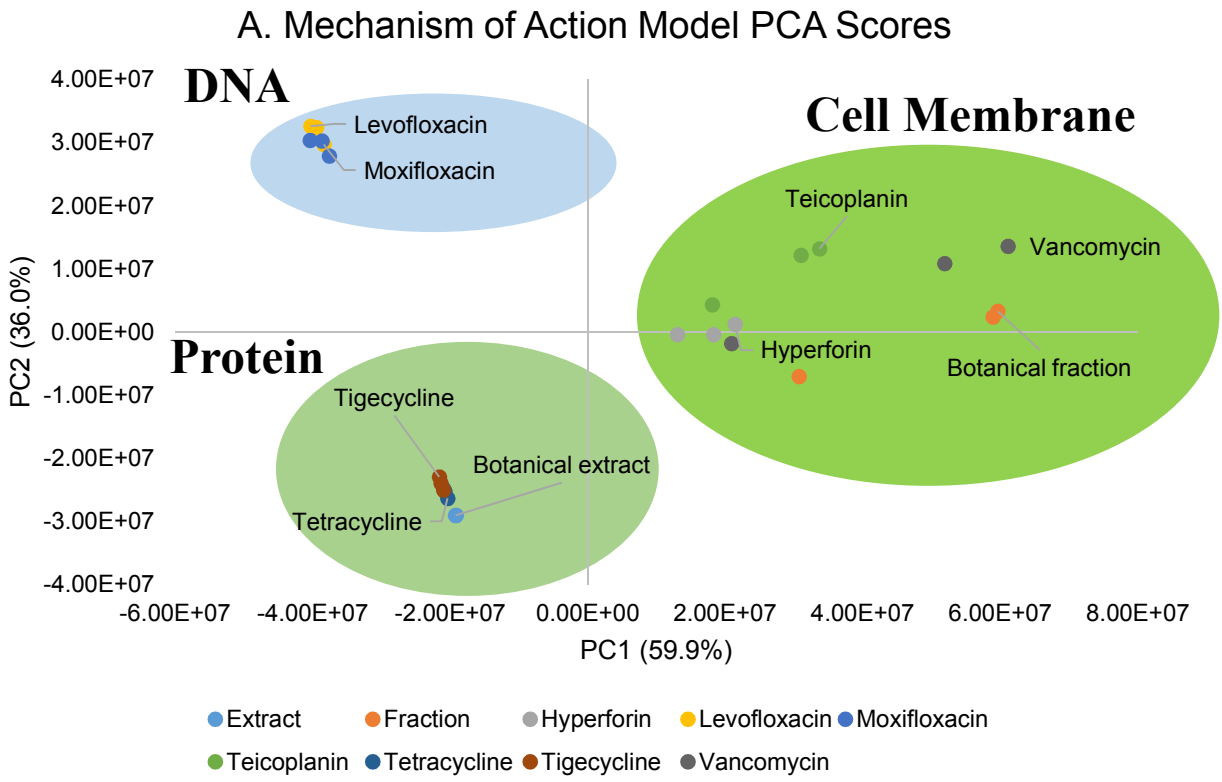

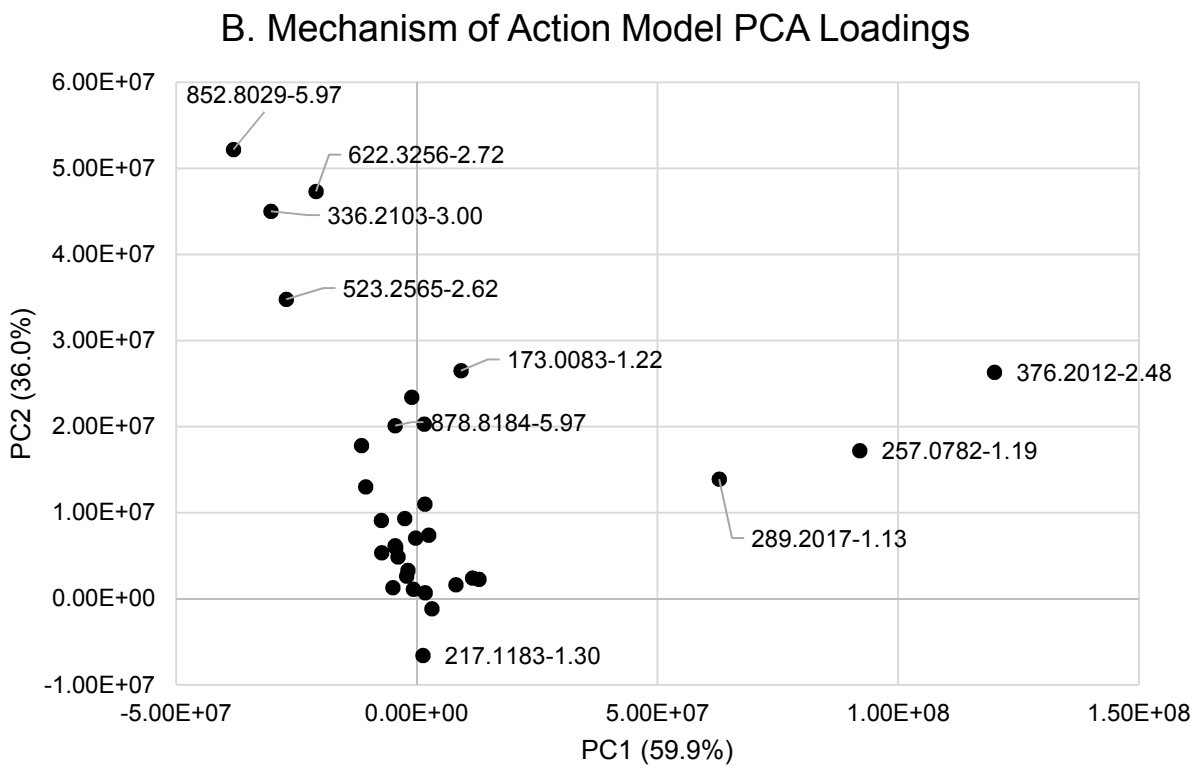

Notes. Mechanism of action model principal component analysis (PCA) scores (A) and loadings (B) plots of extracellular matrices of MRSA after exposure to sublethal concentrations of antibiotics, *H. calycinum* extract, fraction 1 and known botanical compound hyperforin. Clustering samples are grouped in ovals and labeled in bold by antibiotic classification.

Intuition of chemical classifications of the features predicted to be associated with antimicrobial activity in ***Antimicrobial Annotation***, knowledge of tentative and reported antimicrobial compound classes present in the *H. calycinum* samples used in these studies and reported as known to *Hypericum* sp. (116), including xanthones, flavonoids, and phloroglucinols, some hypotheses may be developed on antimicrobial compound classifications and previously reported associated mechanisms of action. Previous literature reports regarding xanthones include the study of α-mangostin (MIC of 1.56 µg/mL against MRSA), its synthetic analogues and related naturally occurring related xanthones acting via a cell membrane disruption mechanism against MRSA (55, 116, 117). Flavonoids, particularly catechins found in *H.*

calycinum, may be synergists to cell wall disruptors **(88, 106, 107)**. Phloroglucinols, and specifically the subclass of acylphloroglucinols, showed widespread antimicrobial activity against MRSA (116, 118). Multiple antimicrobial mechanisms of action are also exhibited by phloroglucinols including disruption of processes related to cell membrane such as depolarization and permeability effects, and cell lysis, though they also target DNA and proteins, influence production of radical oxygen species, disrupt key enzyme sites, and some may interfere with of biofilms (119). The diversity of antimicrobial compounds belonging to multiple classes leads to an expectation that the botanical may similarly exert activity by multiple mechanisms of action.

Evaluation of the prediction model in **Fig. 2.7** reveals the botanical fraction 1 and hyperforin clustering with cell wall disrupting antibiotics. The prediction of hyperforin aligns with literature precedent described above of possible phloroglucinol mechanisms of action. Interestingly, the prediction of the whole extract acting by a mechanism clustering with protein synthesis inhibitors suggests that compounds driving the activity of the whole extract may be operating differently than those driving the activity of its derived fraction 1. Future inclusion of the active fraction 3 in this mechanism of action prediction model would provide further information on the distribution of compounds potentially acting by varied mechanisms. Isolation of all predicted antimicrobial compounds and inclusion in the mechanism of action model alongside the active extract and fractions would aid in clarifying the complex interactions within the botanical samples.

Additional studies to validate the proposed mechanism of action predictions and confirm these predictions include phenotypic target-based assays, quantifying radiolabeled biosynthetic precursors, ligand binding affinity chromatography, resistance profiling after bacterial exposure

to treatment, screening against libraries of bacterial mutants and knockouts, cytological profiling, and transcriptome analyses (120).

MATERIALS AND METHODS

Plant Material

Hypericum calycinum (creeping St. John's Wort) of the family Hypericaceae was collected mid-May on the UNC Greensboro campus in Greensboro, NC and a pressed voucher specimen was retained for submission to the UNC Chapel Hill Herbarium (**Fig. 2.8**).

Fig. 2.8 Photograph of *H. calycinum* plant used to prepare voucher specimen.

Extraction and Fractionation

Newly harvested *H. calycinum* aerial portions were dried on the bench top at 25°C for ~two weeks. The dried material (266 g) was ground using an IKA®-Werke M20 Universal Mill and percolated in ACS grade MeOH at 160 g/L for 24 hr. Liquid extraction was performed using previously described methods (18, 121). The resulting MeOH extract was vacuum filtered off the plant material and rotovapped to dryness. Dried extract was stored at 4°C and plant material was resubmerged in MeOH at 160 g/L, repeated for a total of three extractions of the starting plant material. The combined MeOH extract was concentrated under a stream of nitrogen gas and then further partitioned. A first partition was collected by solubilizing the MeOH extract in a solution of 10% water and MeOH with neat Hexane (1:1). The hexane layer was dried by rotovapping

and stored at -20°C. The aqueous MeOH layer was drawn off with a separatory funnel and dried by rotovapping, then subject to further partitioning in EtOAc/MeOH/H2O (4:5:1). The EtOAc layer was collected and a 1% NaCl solution was added to remove hydrosoluble tannins. Each resulting partitioned layer was dried under a stream of nitrogen gas and yielded 48 g of dried EtOAc extract (18013-164-1A) and stored at -20°C.

A 1.42 g sample of the EtOAc partition was separated by flash chromatography using a 43.4 min (77.5 CV) normal-phase gradient with a RediSep Silica 12 g Gold Column on a Teledyne ISCO Combiflash Rf with evaporative-light scattering detector (ELSD) and a photodiode array (PDA) detector, at 254 nm and 280 nm. The gradient with a 30 mL/min flow rate began with a 6.4 min hold at 100% hexane, with a gradual gradient to 100% chloroform over 12.9 min, preceding a gradual gradient to 20:80 MeOH:$CHCl_3$ over 9.4 min and a rapid increase to 100% MeOH over 1.2 min. The gradient was held at 100% methanol for 13.5 min. Fractionated material collected in tubes was pooled into 4 fractions with a 93.18% recovery of starting material.

Ultra-High Performance Liquid Chromatography-Mass Spectrometry (UHPLC-MS)

Mass spectrometry data collection was performed on a Thermo Fisher Scientific Q-Exactive Plus Orbitrap mass spectrometer with electrospray ionization coupled to a Waters Acquity UHPLC column (BEH C18, 1.7 µm, 2.1 × 50 mm, Waters Corporation, Milford, MA, USA). Samples were prepared in Optima grade methanol at a concentration of 0.01 mg/mL. Data were collected in the full scan mode and data dependent tandem MS/MS mode, fragmenting precursor ions selected in a pre-determined inclusion list with a 2.0 *m/z* detection window. The Thermo Q-Exactive Plus mass spectrometer was operated in the positive mode with resolution of 70,000, full scan range of 200-2,000 *m/z*, maximum IT 100 ms, profile spectrum, and normalized

collision energy of 30 eV for the high-energy collision-induced dissociation (HCD). Instrument conditions were as follows: spray voltage 3030.3 V, spray current 21.31 uA, capillary temperature 256.21°C, sheath gas 48.01, auxiliary gas 11.45, sweep gas 2.36, probe heater temperature 349.99°C, and S-Lens RF level set to 50.00.

Column temperature was 40°C and sample temperature was 10°C. UHPLC analysis with a 3 μL injection volume was performed with a 0.3 mL/min flow rate with a binary solvent system including solvent A, water with 0.1% formic acid added, and solvent B, acetonitrile with 0.1% formic acid added.

Antimicrobial Annotation model chromatography

Gradient elution over a total of 8 minutes was performed, where conditions began at 90 % A : 10% B with these starting conditions held for one minute, then to 0 % A : 100 % B over 4 minutes with a 1.5 minute hold, returning to starting conditions for 0.1 minutes and held for 1.4 minutes. Data were analyzed with Thermo Xcalibur, MZmine 2.53 and Sirius 11.5 (Pattern Recognition Systems AS, Bergen, Norway).

Mechanism of Action chromatography

Gradient elution over a total of 6 minutes was performed, where conditions began at 90 % A : 10% B with these starting conditions held for one minute, then to 0 % A : 100 % B over 4 minutes with a 0.5 minute hold, returning to starting conditions for 0.1 minutes and held for 0.4 minutes. All data for both methods were analyzed with Thermo Xcalibur, MZmine 2.53 and Sirius 11.5 (Pattern Recognition Systems AS, Bergen, Norway).

Antimicrobial Evaluation

Extracts, fractions and pure compounds were tested for inhibitory activity against clinically relevant methicillin-resistant *Staphylococcus aureus* (MRSA), strain USA300 LAC AH1263 (15) using Clinical Laboratory Standards Institute (CLSI) guidelines (35). In brief as previously described (17-19, 22), to prepare the bacterial culture, a swab of cryopreserved stock of MRSA was T-streaked and incubated upon Tryptic Soy agar at 37°C in a humid environment for 18 h. A single colony was inoculated into 5 mL of Tryptic Soy broth and incubated at 37°C, shaking at 250 rpm for 18 h. A seed culture was started two hours prior to addition to 96-well microplate by diluting the inoculum into a total volume of 15 mL of Tryptic Soy broth. The OD_{600} value of this culture was measured with a Synergy H1 microplate reader (Biotek, Winooski, VT, USA) and the culture was adjusted to 5×10^5 colony forming units (CFU)/mL. Each well was uniformly inoculated with this standardized bacterial culture and co-incubated with vehicle control of 2% DMSO, positive control levofloxacin at 10 μg/mL (Sigma-Aldrich), or test compounds in 2% DMSO. Test compounds were prepared in an 8-point 2-fold dilution series ranging from 0 to 10 μg/mL and added to the 96-well microplate in triplicate, as well as duplicated in a control plate with no bacterial organism inoculation used for subtraction of any absorbance readings resulting from extracts and compounds. Percent inhibition of growth was calculated in Excel as ((average OD_{600} of vehicle control – OD_{600} of one biological replicate) / average OD_{600} of vehicle control) * 100. An average of biological triplicates was plotted, and error bars represent a calculation of the standard error of the mean. The inhibitory concentration at half-maximal growth (IC_{50}) was calculated using nonlinear regression analysis of the inhibitory dose-response curve from OD_{600} readings, stock concentrations and error (manually calculated as standard error of the mean) in GraphPad Prism version 9.3.1 software.

Mechanism of Action Antimicrobial Assay

Techniques described above in ***Antimicrobial Evaluation*** were performed to prepare an antimicrobial sample set for mechanism of action determination with the following modifications. After collecting OD_{600} absorbance readings, bacterial cells were removed from all sample wells with sterile 0.22-µm-pore hydrophilic low protein binding Durapore® membrane 96-well filter plates (Merck Millipore) under vacuum as previously described (21, 122). Retained extracellular matrices were stored at -20°C prior to mass spectrometry analyses. All sample conditions were performed with five replicates, duplicated in a plate with bacterial organism inoculation and a control plate with no bacterial organism inoculation, used for subtraction of any absorbance readings resulting from extracts and compounds. Absorbance OD_{600} readings were processed against the background subtraction control plate. Average growth and standard error of the mean were calculated. The five biological replicates were evaluated for outliers by performance of a Grubbs' test with 95% confidence for removal of values > 1.672 with five observations as compared to the other replicates in each sample set (123).

Biochemometric Analyses

Previously developed workflows were adapted to evaluate *H. calycinum* by OPLS-DA regression modeling and mechanism of action prediction (17, 19). MZmine 2.53 was used to filter raw UHPLC-MS files (124). Data filtering techniques were applied and described in Table 2.1. Additional filtering was applied to each model as follows.

Antimicrobial Annotation Model: positive and negative ionization mode data were first merged into a data set of 8,081 features. Next, a 30% relative standard deviation (RSD) threshold was applied to all features, retaining features scoring greater than 30%. Features present in the methanol blank were next removed if the percent ratio compared to all other samples was greater

than 80%. After filtering blanks, 6,936 features remained. A 35% RSD filter was applied to triplicate sample peak areas. A final variance filter was applied with a cutoff of 0.01% of the features with the greatest level of variance, leaving 314 features used to model the partial least squares (PLS) scores and loadings plots. These features were further used to model the selectivity ratio (SR) analysis including % inhibition with validation by mean centring, leaving out every one object with 100 iterations, significance level 0.5 to generate 3 components. A 0.01% variance cutoff was applied and component 1 was visualized.

Mechanism of Action Model: positive and negative ionization mode data were first merged into a data set of 8,900 features. Samples were next selected by randomization to reduce the sample set from five replicates to three replicates of each treatment. Next, a 30% relative standard deviation (RSD) threshold was applied to all features, retaining features scoring greater than 30%. Features present in the methanol blank were next removed if the percent ratio compared to all other samples was greater than 80%. Identical 80% percent ratio feature removal filters were applied by comparison to the Mueller-Hinton broth control, then the Mueller-Hinton broth with 2% DMSO vehicle control. After filtering blanks, 1,066 features remained. A 35% RSD filter was applied to triplicate sample peak areas. A reference blank 80% ratio filter was applied to each triplicate set of samples to remove signals in the antibiotic, extract, fraction or pure compound mixtures. An 80% ratio filter was applied to remove signals in a bacterial growth control, and subsequently an 80% ratio filter to remove signals from the bacterial growth control with 2% DMSO vehicle. An additional filtering strategy was applied to visualize the mechanism of action prediction model, by assessing the presence or absence of features uniquely appearing in antibiotics belonging to the same mechanism. This strategy was applied to all samples in the

data set and 32 features uniquely appearing in samples acting via the same mechanism of action were plotted using principal component analysis (PCA) scores and loadings modeling in **Fig. 2.7**.

Table 2.1 Summary of metabolomics data processing parameters for both the mechanism of action and antimicrobial annotation studies.

UHPLC-MS (124)	Mechanism of Action Model	Antimicrobial Annotation Model
A. Crop Filter		
RT range	1.00 to 6.00	1.00 to 8.00
MS level	1	1
Polarity	POS & NEG	POS & NEG
Spectrum type	Centroid	Centroid
Mass range	Auto range	Auto range
B. Mass Detection		
Spectrum type	Centroid	Profile
Noise level	1.00E+04	5.00E+04
C. ADAP Chromatogram Builder		
No. of scans	5	5
Group Intensity Threshold	5.00E+04	5.00E+03
Min Highest Intensity	1.00E+06	5.00E+05
m/z tolerance	0.003 Da	0.003 Da
D. Wavelets ADAP Deconvolution		
S/N threshold	10	10
m/z center calculation	Median	Median
S/N estimator	Intense window	Intense window
Minimum Feature Height	5.00E+05	5.00E+04
Coefficient/Area Threshold	50	50
Peak Duration Range	0.00-2.00	0.00 to 1.00
RT Wavelet Range	0-0.10	0.00 to 0.10
E. Isotopic Peaks Grouper		
m/z tolerance	0.0015 Da	0.0015 Da
RT tolerance	0.05	0.05
Maximum charge	3	3
Representative isotope	Most intense	Most intense
F. Join Aligner		
m/z tolerance	0.0015 Da	0.0015 Da
Weight for *m/z*	2	2
RT tolerance	0.05	0.05
Weight for RT	1	1
Require same charge state	checked	checked
Compare isotope pattern	checked	checked

Isotope *m/z* tolerance	0.0015 Da	0.0015 Da
Min absolute intensity	1.00E+04	5.00E+04
Min score	50%	50%
G. Gap Filling Same RT and *m/z*		
m/z tolerance	0.0015 Da	0.0015 Da
H. Duplicate Peak Filter		
Filter mode	New average	New average
m/z tolerance	0.0015 Da	0.0015 Da
RT tolerance	0.05	0.05
I. Peak Filter		
Height	1E5 to 1E10	5E4 to 1E10
No. of Data Points	4 to 300	4 to 300

CHAPTER III: CONCLUDING REMARKS

Collectively, the results presented in the first study support the use of phenotypic screening of existing libraries against high priority bacterial pathogens to yield promising avenues for antimicrobial development. While much of the research that is accomplished in the field of natural products drug discovery focuses on discovery of new chemical entities, we should not lose site of the potential value of identifying known compounds with promising new activities. It is also useful to remember that the "tried and true" methods that served as a basis for antimicrobial lead discovery in the 1940s, 50s and 60s may still be useful today, especially as a preliminary rapid screening step prior to more quantitative approaches. With regards to this specific study, the use of a plate-based assay enabled rapid screening of a large number (2,500) extracts, with very little cost, and ultimately produced a lead compound that shows promise against the high priority pathogen *A. baumannii*.

Antimicrobial mechanisms of action of complex antimicrobial extracts in the second studies were predicted using a metabolomics approach. An extract of *H. calycinum* and its active fraction, with a standard of hyperforin, were classified as acting by protein synthesis inhibition and cell wall disruption mechanisms of action, respectively in comparison to six clinically relevant antibiotics representing three mechanisms of action. Further studies to annotate the features contributing to mechanism of action classification and link to biological pathways are needed, as well as validation of the mechanism of action of this botanical species against MRSA.

REFERENCES

1. CDC. 2019. Leading causes of Death, 1900-1998. National Center for Health Statistics:1-67.
2. Armitage EG, Godzien J, Pena I, Lopez-Gonzalvez A, Angulo S, Gradillas A, Alonso-Herranz V, Martin J, Fiandor JM, Barrett MP, Gabarro R, Barbas C. 2018. Metabolic Clustering Analysis as a Strategy for Compound Selection in the Drug Discovery Pipeline for Leishmaniasis. *ACS Chem Biol* 13:1361-1369.
3. Johnston CW, Skinnider MA, Dejong CA, Rees PN, Chen GM, Walker CG, French S, Brown ED, Berdy J, Liu DY, Magarvey NA. 2016. Assembly and clustering of natural antibiotics guides target identification. Nat Chem Biol 12:233-9.
4. Ochoa JL, Bray WM, Lokey RS, Linington RG. 2015. Phenotype-Guided Natural Products Discovery Using Cytological Profiling. *J Nat Prod* 78:2242-8.
5. Subramanian A, Narayan R, Corsello SM, Peck DD, Natoli TE, Lu X, Gould J, Davis JF, Tubelli AA, Asiedu JK, Lahr DL, Hirschman JE, Liu Z, Donahue M, Julian B, Khan M, Wadden D, Smith IC, Lam D, Liberzon A, Toder C, Bagul M, Orzechowski M, Enache OM, Piccioni F, Johnson SA, Lyons NJ, Berger AH, Shamji AF, Brooks AN, Vrcic A, Flynn C, Rosains J, Takeda DY, Hu R, Davison D, Lamb J, Ardlie K, Hogstrom L, Greenside P, Gray NS, Clemons PA, Silver S, Wu X, Zhao WN, Read-Button W, Wu X, Haggarty SJ, Ronco LV, Boehm JS, et al. 2017. A Next Generation Connectivity Map: L1000 Platform and the First 1,000,000 Profiles. *Cell* 171:1437-1452.e17.
6. Martens E, Demain AL. 2017. The antibiotic resistance crisis, with a focus on the United States. J Antibiot (Tokyo) 70:520-526.

7. Hiltunen T, Virta M, Laine AL. 2017. Antibiotic resistance in the wild: an eco-evolutionary perspective. Philos Trans R Soc Lond B Biol Sci 372.

8. Jacobs AC, Thompson MG, Black CC, Kessler JL, Clark LP, McQueary CN, Gancz HY, Corey BW, Moon JK, Si Y, Owen MT, Hallock JD, Kwak YI, Summers A, Li CZ, Rasko DA, Penwell WF, Honnold CL, Wise MC, Waterman PE, Lesho EP, Stewart RL, Actis LA, Palys TJ, Craft DW, Zurawski DV. 2014. AB5075, a Highly Virulent Isolate of Acinetobacter baumannii, as a Model Strain for the Evaluation of Pathogenesis and Antimicrobial Treatments. MBio 5:e01076-14.

9. Quandt CA, Kepler RM, Gams W, Araújo JPM, Ban S, Evans HC, Hughes D, Humber R, Hywel-Jones N, Li Z, Luangsa-ard JJ, Rehner SA, Sanjuan T, Sato H, Shrestha B, Sung G-H, Yao Y-J, Zare R, Spatafora JW. 2014. Phylogenetic-based nomenclatural proposals for *Ophiocordycipitaceae* (Hypocreales) with new combinations in *Tolypocladium*. *IMA Fungus* 5:121-134.

10. Teshima Y, Shin-ya K, Shimazu A, Furihata K, Chul HS, Furihata K, Hayakawa Y, Nagai K, Seto H. 1991. Isolation and structural elucidation of pyridoxatin, a free radical scavenger of microbial origin. *J Antibiot* (Tokyo) 44:685-7.

11. Marik T, Tyagi C, Balazs D, Urban P, Szepesi A, Bakacsy L, Endre G, Rakk D, Szekeres A, Andersson MA, Salonen H, Druzhinina IS, Vagvolgyi C, Kredics L. 2019. Structural Diversity and Bioactivities of Peptaibol Compounds From the Longibrachiatum Clade of the Filamentous Fungal Genus Trichoderma. Front Microbiol 10:1434.

12. Meir M, Grosfeld T, Barkan D. 2018. Establishment and Validation of Galleria mellonella as a Novel Model Organism To Study Mycobacterium abscessus Infection, Pathogenesis, and Treatment. Antimicrob Agents Chemother 62.

13. Huggins WM, Minrovic BM, Corey BW, Jacobs AC, Melander RJ, Sommer RD, Zurawski DV, Melander C. 2017. 1,2,4-Triazolidine-3-thiones as Narrow Spectrum Antibiotics against Multidrug-Resistant Acinetobacter baumannii. ACS Med Chem Lett 8:27-31.

14. Gupta PD, Birdi TJ. 2017. Development of botanicals to combat antibiotic resistance. *J Ayurveda Integr Med* 8:266-275.

15. Boles BR, Thoendel M, Roth AJ, Horswill AR. 2010. Identification of Genes Involved in Polysaccharide-Independent *Staphylococcus aureus* Biofilm Formation. *PLOS ONE* 5:e10146.

16. Schempp CM, Pelz K, Wittmer A, Schöpf E, Simon JC. 1999. Antibacterial activity of hyperforin from St John's wort, against multiresistant *Staphylococcus aureus* and gram-positive bacteria. *The Lancet* 353:2129.

17. Caesar LK, Kellogg JJ, Kvalheim OM, Cech NB. 2019. Opportunities and Limitations for Untargeted Mass Spectrometry Metabolomics to Identify Biologically Active Constituents in Complex Natural Product Mixtures. *J Nat Prod* 82:469-484.

18. Caesar LK, Kellogg JJ, Kvalheim OM, Cech RA, Cech NB. 2018. Integration of Biochemometrics and Molecular Networking to Identify Antimicrobials in *Angelica keiskei*. *Planta Med* 84:721-728.

19. Kellogg JJ, Todd DA, Egan JM, Raja HA, Oberlies NH, Kvalheim OM, Cech NB. 2016. Biochemometrics for Natural Products Research: Comparison of Data Analysis Approaches and Application to Identification of Bioactive Compounds. *J Nat Prod* 79:376-86.

20. Kellogg JJ, Paine MF, McCune JS, Oberlies NH, Cech NB. 2019. Selection and characterization of botanical natural products for research studies: a NaPDI center recommended approach. Nat Prod Rep doi:10.1039/c8np00065d.

21. Todd DA, Zich DB, Ettefagh KA, Kavanaugh JS, Horswill AR, Cech NB. 2016. Hybrid Quadrupole-Orbitrap mass spectrometry for quantitative measurement of quorum sensing inhibition. *J Microbiol Methods* 127:89-94.

22. Britton ER, Kellogg JJ, Kvalheim OM, Cech NB. 2018. Biochemometrics to Identify Synergists and Additives from Botanical Medicines: A Case Study with *Hydrastis canadensis* (Goldenseal). *J Nat Prod* 81:484-493.

23. Aminov RI. 2010. A brief history of the antibiotic era: lessons learned and challenges for the future. Front Microbiol 1:134.

24. Tippett R. 2014. Mortality and Cause of Death, 1900 v. 2010.

25. WHO. 2017. Critically Important Antimicrobials for Human Medicine - 5th rev.

26. Maragakis LL, Perl TM. 2008. Acinetobacter baumannii: epidemiology, antimicrobial resistance, and treatment options. Clin Infect Dis 46:1254-63.

27. Zaidan N, Hornak JP, Reynoso D. 2021. Extensively Drug-Resistant *Acinetobacter baumannii* Nosocomial Pneumonia Successfully Treated with a Novel Antibiotic Combination. *Antimicrob Agents Chemother* 65:e0092421.

28. Tacconelli E, Carrara E, Savoldi A, Harbarth S, Mendelson M, Monnet DL, Pulcini C, Kahlmeter G, Kluytmans J, Carmeli Y, Ouellette M, Outterson K, Patel J, Cavaleri M, Cox EM, Houchens CR, Grayson ML, Hansen P, Singh N, Theuretzbacher U, Magrini N. 2018. Discovery, research, and development of new antibiotics: the WHO priority list of antibiotic-resistant bacteria and tuberculosis. Lancet Infect Dis 18:318-327.

29. CDC. 2019. Antibiotic Resistance Threats in the United States, 2019., Atlanta, GA: U.S. Department of Health and Human Services, CDC; 2019.

30. Nowak P, Paluchowska P. 2016. Acinetobacter baumannii: biology and drug resistance - role of carbapenemases. Folia Histochem Cytobiol 54:61-74.

31. Ribeiro da Cunha B, Fonseca LP, Calado CRC. 2019. Antibiotic Discovery: Where Have We Come from, Where Do We Go? *Antibiotics* (Basel) 8.

32. Davis RL. 2020. Mechanism of Action and Target Identification: A Matter of Timing in Drug Discovery. *iScience* 23:101487.

33. Swinney DC, Anthony J. 2011. How were new medicines discovered? *Nat Rev Drug Discov* 10:507-19.

34. Rivera-Chávez J, El-Elimat T, Gallagher JM, Graf TN, Fournier J, Panigrahi GK, Deep G, Bunch RL, Raja HA, Oberlies NH. 2019. Delitpyrones: α-Pyrone Derivatives from a Freshwater *Delitschia* sp. *Planta Med* 85:62-71.

35. CLSI. 2022. Clinical and Laboratory Standards Institute. Performance Standards for Antimicrobial Susceptibility Testing, vol 32nd ed.

36. Paguigan ND, El-Elimat T, Kao D, Raja HA, Pearce CJ, Oberlies NH. 2017. Enhanced dereplication of fungal cultures via use of mass defect filtering. J Antibiot (Tokyo) 70:553-561.

37. El-Elimat T, Figueroa M, Ehrmann BM, Cech NB, Pearce CJ, Oberlies NH. 2013. High-resolution MS, MS/MS, and UV database of fungal secondary metabolites as a dereplication protocol for bioactive natural products. *J Nat Prod* 76:1709-16.

38. Salvi A, Amrine CSM, Austin JR, Kilpatrick K, Russo A, Lantvit D, Calderon-Gierszal E, Mattes Z, Pearce CJ, Grinstaff MW, Colby AH, Oberlies NH, Burdette JE. 2020. Verticillin

A Causes Apoptosis and Reduces Tumor Burden in High-Grade Serous Ovarian Cancer by Inducing DNA Damage. *Mol Cancer Ther* 19:89-100.

39. Lee h-J, Myung-Chul Chung, Choong-Hwan Lee, Hyo-Kon Chun, Hwan-Mook Kim, Yung-Hee Kho. 1996. Pyridoxatin, an Inhibitor of Gelatinase A with Cytotoxic Activity. *J Microbiol Biotechnol* 6:445-450.

40. Barry B. Snider QL. 1994. Total Synthesis of (+/-)-Pyridoxatin. *J Org Chem* 59:8065-8070.

41. Zhang S-H, Yue X-L, Zhao X, Tang J, Yang Y, Xu R, Ma H, Zhu S-M, Luo F-Y, Zhang Q, Zhang G-G, Li C-W. 2022. Longibrachiamide A, a 20-Residue Peptaibol Isolated from *Trichoderma longibrachiatum* Rifai DMG-3-1-1. *Chem Biodivers* 19:e202200286.

42. Mikkola R, Andersson MA, Kredics L, Grigoriev PA, Sundell N, Salkinoja-Salonen MS. 2012. 20-Residue and 11-residue peptaibols from the fungus Trichoderma longibrachiatum are synergistic in forming Na+/K+ -permeable channels and adverse action towards mammalian cells. Febs j 279:4172-90.

43. Castagnoli E, Marik T, Mikkola R, Kredics L, Andersson MA, Salonen H, Kurnitski J. 2018. Indoor Trichoderma strains emitting peptaibols in guttation droplets. J Appl Microbiol 125:1408-1422.

44. Khalil ZG, Salim AA, Lacey E, Blumenthal A, Capon RJ. 2014. Wollamides: antimycobacterial cyclic hexapeptides from an Australian soil *Streptomyces*. *Org Lett* 16:5120-3.

45. Cai F, Druzhinina IS. 2021. In honor of John Bissett: authoritative guidelines on molecular identification of *Trichoderma*. *Fungal Divers* 107:1-69.

46. Jaklitsch WM. 2011. European species of *Hypocrea* part II: species with hyaline ascospores. *Fungal Divers* 48:1-250.

47. Jaklitsch WM, Voglmayr H. 2015. Biodiversity of *Trichoderma* (Hypocreaceae) in Southern Europe and Macaronesia. *Stud Mycol* 80:1-87.

48. Raja HA, Miller AN, Pearce CJ, Oberlies NH. 2017. Fungal Identification Using Molecular Tools: A Primer for the Natural Products Research Community. *J Nat Prod* 80:756-770.

49. Ten KE, Md Zoqratt MZH, Ayub Q, Tan HS. 2021. Characterization of multidrug-resistant Acinetobacter baumannii strain ATCC BAA1605 using whole-genome sequencing. BMC Res Notes 14:83.

50. Wu B, Oesker V, Wiese J, Schmaljohann R, Imhoff JF. 2014. Two new antibiotic pyridones produced by a marine fungus, *Trichoderma* sp. strain MF106. *Mar Drugs* 12:1208-19.

51. Dorsaz S, Snaka T, Favre-Godal Q, Maudens P, Boulens N, Furrer P, Ebrahimi SN, Hamburger M, Allemann E, Gindro K, Queiroz EF, Riezman H, Wolfender JL, Sanglard D. 2017. Identification and Mode of Action of a Plant Natural Product Targeting Human Fungal Pathogens. *Antimicrob Agents Chemother* 61.

52. Chang W, Zhang M, Li Y, Li X, Gao Y, Xie Z, Lou H. 2015. Lichen endophyte derived pyridoxatin inactivates *Candida* growth by interfering with ergosterol biosynthesis. *Biochim Biophys Acta* 1850:1762-71.

53. Leitgeb B, Szekeres A, Manczinger L, Vágvölgyi C, Kredics L. 2007. The history of alamethicin: a review of the most extensively studied peptaibol. *Chem Biodivers* 4:1027-51.

54. Richardson H, Emslie-Smith AH, Senior BW. 1968. Agar diffusion method for the assay of colicins. Appl Microbiol 16:1468-74.

55. Vilgalys R, Hester M. 1990. Rapid genetic identification and mapping of enzymatically amplified ribosomal DNA from several *Cryptococcus* species. *J Bacteriol* 172:4238-46.

56. Rehner SA, Samuels GJ. 1995. Molecular systematics of the *Hypocreales*: a teleomorph gene phylogeny and the status of their anamorphs. Canad J Bot 73:816-823.

57. Raja HA, Baker TR, Little JG, Oberlies NH. 2017. DNA barcoding for identification of consumer-relevant mushrooms: A partial solution for product certification? *Food Chem* 214:383-392.

58. Montalva C, Silva JJ, Rocha LFN, Luz C, Humber RA. 2019. Characterization of *Tolypocladium cylindrosporum* (Hypocreales, Ophiocordycipitaceae) isolates from Brazil and their efficacy against *Aedes aegypti* (Diptera, Culicidae). *J Appl Microbiol* 126:266-276.

59. Edgar RC. 2004. MUSCLE: multiple sequence alignment with high accuracy and high throughput. *Nucleic Acids Res* 32:1792-7.

60. Gouy M, Guindon S, Gascuel O. 2010. SeaView version 4: A multiplatform graphical user interface for sequence alignment and phylogenetic tree building. *Mol Biol Evol* 27:221-4.

61. Li XB, Li L, Zhu RX, Li W, Chang WQ, Zhang LL, Wang XN, Zhao ZT, Lou HX. 2015. Tetramic Acids and Pyridone Alkaloids from the Endolichenic Fungus *Tolypocladium cylindrosporum*. *J Nat Prod* 78:2155-60.

62. White TJ, Bruns T, Lee SH, Taylor JW (ed). 1990. PCR protocols: a guide to methods and application. San Diego.

63. Gardes M, White TJ, Fortin JA, Bruns TD, Taylor JW. 1991. Identification of Indigenous and Introduced Symbiotic Fungi in Ectomycorrhizae by Amplification of Nuclear and Mitochondrial Ribosomal DNA. Can J Bot 69:180-190.

64. Carbone I, Kohn LM. 1999. A method for designing primer sets for speciation studies in filamentous ascomycetes. Mycologia:553-556.

65. Jaklitsch WM, Komon M, Kubicek CP, Druzhinina IS. 2005. Hypocrea voglmayrii sp. nov. from the Austrian Alps represents a new phylogenetic clade in Hypocrea/Trichoderma. Mycologia 97:1365-1378.

66. Ayers S, Graf TN, Adcock AF, Kroll DJ, Shen Q, Swanson SM, Matthew S, De Blanco EJC, Wani MC, Darveaux BA. 2012. Cytotoxic xanthone–anthraquinone heterodimers from an unidentified fungus of the order *Hypocreales* (MSX 17022). *J Antibiot* (Tokyo) 65:3-8.

67. Rivera-Chávez J, Raja HA, Graf TN, Gallagher JM, Metri P, Xue D, Pearce CJ, Oberlies NH. 2017. Prealamethicin F50 and related peptaibols from Trichoderma arundinaceum: Validation of their authenticity via in situ chemical analysis. RSC Adv 7:45733-45751.

68. Figueroa M, Raja H, Falkinham JO, 3rd, Adcock AF, Kroll DJ, Wani MC, Pearce CJ, Oberlies NH. 2013. Peptaibols, tetramic acid derivatives, isocoumarins, and sesquiterpenes from a *Bionectria* sp. (MSX 47401). *J Nat Prod* 76:1007-15.

69. Jaiswal Y, Liang Z, Zhao Z. 2016. Botanical drugs in Ayurveda and Traditional Chinese Medicine. *J Ethnopharmacol* 194:245-259.

70. Clarke TC, Black LI, Stussman BJ, Barnes PM, Nahin RL. 2015. Trends in the use of complementary health approaches among adults: United States, 2002-2012. *Natl Health Stat Report*:1-16.

71. Schmidt B, Ribnicky DM, Poulev A, Logendra S, Cefalu WT, Raskin I. 2008. A natural history of botanical therapeutics. *Metabolism* 57:S3-9.

72. Cowan MM. 1999. Plant products as antimicrobial agents. *Clin Microbiol Rev* 12:564-82.

73. Farnsworth NR, Morris RW. 1976. Higher plants--the sleeping giant of drug development. *Am J Pharm Sci Support Public Health* 148:46-52.

74. Anonymous. https://www.fda.gov/food/food-labeling-nutrition/structurefunction-claims (14 December 2017). U.S. Food & Drug Adminstration: Structure/Function Claims.

75. Feher M, Schmidt JM. 2003. Property distributions: differences between drugs, natural products, and molecules from combinatorial chemistry. *J Chem Inf Comput Sci* 43:218-27.

76. Lee ML, Schneider G. 2001. Scaffold architecture and pharmacophoric properties of natural products and trade drugs: application in the design of natural product-based combinatorial libraries. *J Comb Chem* 3:284-9.

77. Koch MA, Schuffenhauer A, Scheck M, Wetzel S, Casaulta M, Odermatt A, Ertl P, Waldmann H. 2005. Charting biologically relevant chemical space: a structural classification of natural products (SCONP). *Proc Natl Acad Sci U S A* 102:17272-7.

78. Htoo HH, Brumage L, Chaikeeratisak V, Tsunemoto H, Sugie J, Tribuddharat C, Pogliano J, Nonejuie P. 2019. Bacterial Cytological Profiling as a Tool To Study Mechanisms of Action of Antibiotics That Are Active against *Acinetobacter baumannii*. *Antimicrob Agents Chemother* 63.

79. Schenone M, Dancik V, Wagner BK, Clemons PA. 2013. Target identification and mechanism of action in chemical biology and drug discovery. *Nat Chem Biol* 9:232-40.

80. Wang XJ, Ren JL, Zhang AH, Sun H, Yan GL, Han Y, Liu L. 2019. Novel applications of mass spectrometry-based metabolomics in herbal medicines and its active ingredients: Current evidence. *Mass Spectrom Rev* 38:380-402.

81. Gronquist M, Bezzerides A, Attygalle A, Meinwald J, Eisner M, Eisner T. 2001. Attractive and defensive functions of the ultraviolet pigments of a flower (*Hypericum calycinum*). *Proc Natl Acad Sci U S A* 98:13745-50.

82. Oztürk Y, Aydin S, Beis R, Başer KH, Berberoĝlu H. 1996. Effects of *Hypericum perforatum* L. and *Hypericum calycinum* L. extracts on the central nervous system in mice. *Phytomedicine* 3:139-46.

83. Win T, Htwe TT, Shwe HH, Heilmann J. 2012. Lavandulyl flavanones from the stems of *Hypericum calycinum* L. *Chem Biodivers* 9:1198-204.

84. Maggi F, Cecchini C, Cresci A, Coman MM, Tirillini B, Sagratini G, Papa F, Vittori S. 2010. Chemical composition and antimicrobial activity of the essential oils from several Hypericum taxa (Guttiferae) growing in central Italy (Appennino Umbro-Marchigiano). *Chem Biodivers* 7:447-66.

85. Vestergaard M, Frees D, Ingmer H. 2019. Antibiotic Resistance and the MRSA Problem. *Microbiology Spectrum* 7:7.2.18.

86. Kirmizibekmez H, Bassarello C, Piacente S, Celep E, Atay I, Mercanoğlu G, Yeşilada E. 2009. Phenolic compounds from *Hypericum calycinum* and their antioxidant activity. *Nat Prod Commun* 4:531-4.

87. Pytlakowska K, Kita A, Janoska P, Połowniak M, Kozik V. 2012. Multi-element analysis of mineral and trace elements in medicinal herbs and their infusions. *Food Chem* 135:494-501.

88. Cirak C, Radusiene J, Jakstas V, Ivanauskas L, Seyis F, Yayla F. 2016. Secondary metabolites of seven *Hypericum* species growing in Turkey. *Pharm Biol* 54:2244-53.

89. Napoli E, Siracusa L, Ruberto G, Carrubba A, Lazzara S, Speciale A, Cimino F, Saija A, Cristani M. 2018. Phytochemical profiles, phototoxic and antioxidant properties of eleven *Hypericum* species - A comparative study. *Phytochemistry* 152:162-173.

90. Boubakir Z, Beuerle T, Liu B, Beerhues L. 2005. The first prenylation step in hyperforin biosynthesis. *Phytochemistry* 66:51-7.

91. Klingauf P, Beuerle T, Mellenthin A, El-Moghazy SA, Boubakir Z, Beerhues L. 2005. Biosynthesis of the hyperforin skeleton in *Hypericum calycinum* cell cultures. *Phytochemistry* 66:139-45.

92. Gaid MM, Sircar D, Müller A, Beuerle T, Liu B, Ernst L, Hänsch R, Beerhues L. 2012. Cinnamate:CoA ligase initiates the biosynthesis of a benzoate-derived xanthone phytoalexin in *Hypericum calycinum* cell cultures. *Plant Physiol* 160:1267-80.

93. Fiesel T, Gaid M, Müller A, Bartels J, El-Awaad I, Beuerle T, Ernst L, Behrends S, Beerhues L. 2015. Molecular Cloning and Characterization of a Xanthone Prenyltransferase from *Hypericum calycinum* Cell Cultures. *Molecules* 20:15616-30.

94. El-Awaad I, Bocola M, Beuerle T, Liu B, Beerhues L. 2016. Bifunctional CYP81AA proteins catalyse identical hydroxylations but alternative regioselective phenol couplings in plant xanthone biosynthesis. *Nat Commun* 7:11472.

95. Nagia M, Gaid M, Biedermann E, Fiesel T, El-Awaad I, Hänsch R, Wittstock U, Beerhues L. 2019. Sequential regiospecific gem-diprenylation of tetrahydroxyxanthone by prenyltransferases from *Hypericum* sp. *New Phytol* 222:318-334.

96. Singh P, Preu L, Beuerle T, Kaufholdt D, Hänsch R, Beerhues L, Gaid M. 2020. A promiscuous coenzyme A ligase provides benzoyl-coenzyme A for xanthone biosynthesis in Hypericum. *Plant J* 104:1472-1490.

97. Singh P, Kaufholdt D, Awadalah M, Hänsch R, Beerhues L, Gaid M. 2021. Cytosolic aromatic aldehyde dehydrogenase provides benzoic acid for xanthone biosynthesis in Hypericum. *Plant Physiol Biochem* 160:82-93.

98. Saddiqe Z, Naeem I, Maimoona A. 2010. A review of the antibacterial activity of *Hypericum perforatum* L. *J Ethnopharmacol* 131:511-21.

99. Kubin A, Wierrani F, Burner U, Alth G, Grünberger W. 2005. Hypericin--the facts about a controversial agent. *Curr Pharm Des* 11:233-53.

100. Kellogg JJ, Graf TN, Paine MF, McCune JS, Kvalheim OM, Oberlies NH, Cech NB. 2017. Comparison of Metabolomics Approaches for Evaluating the Variability of Complex Botanical Preparations: Green Tea (Camellia sinensis) as a Case Study. J Nat Prod 80:1457-1466.

101. Wallace ED, Oberlies NH, Cech NB, Kellogg JJ. 2018. Detection of adulteration in *Hydrastis canadensis* (goldenseal) dietary supplements via untargeted mass spectrometry-based metabolomics. *Food Chem Toxicol* 120:439-447.

102. Schymanski EL, Jeon J, Gulde R, Fenner K, Ruff M, Singer HP, Hollender J. 2014. Identifying small molecules via high resolution mass spectrometry: communicating confidence. *Environ Sci Technol* 48:2097-8.

103. Nagai M. 1987. Antimicrobial Compounds, Chinesin I and II from Flowers of Hypericum chinense L. Chem Lett.

104. Decosterd LA, Stoeckli-Evans H, Chapuis J-C, Sordat B, Hostettmann K. 1989. New Cell Growth-Inhibitory Cyclohexadienone Derivatives from Hypericum calycinum L. Helvetica Chimica Acta 72:1833-1845.

105. Osman K, Evangelopoulos D, Basavannacharya C, Gupta A, McHugh TD, Bhakta S, Gibbons S. 2012. An antibacterial from *Hypericum acmosepalum* inhibits ATP-dependent MurE ligase from *Mycobacterium tuberculosis*. *Int J Antimicrob Agents* 39:124-129.

106. Zhang LL, Zhang LF, Xu JG. 2020. Chemical composition, antibacterial activity and action mechanism of different extracts from hawthorn (*Crataegus pinnatifida* Bge.). *Sci Rep* 10:8876.

107. Wu M, Brown AC. 2021. Applications of Catechins in the Treatment of Bacterial Infections. *Pathogens* 10.

108. Abe S, Tanaka N, Kobayashi J. 2012. Prenylated acylphloroglucinols, chipericumins A-D, from *Hypericum chinense*. *J Nat Prod* 75:484-8.

109. Ang CYW, Hu L, Heinze TM, Cui Y, Freeman JP, Kozak K, Luo W, Liu FF, Mattia A, DiNovi M. 2004. Instability of St. John's Wort (*Hypericum perforatum* L.) and Degradation of Hyperforin in Aqueous Solutions and Functional Beverage. *J Agric Food Chem* 52:6156-6164.

110. Fuzzati N, Gabetta B, Strepponi I, Villa F. 2001. High-performance liquid chromatography–electrospray ionization mass spectrometry and multiple mass spectrometry studies of hyperforin degradation products. *Journal of Chromatography A* 926:187-198.

111. Schiavone BI, Rosato A, Marilena M, Gibbons S, Bombardelli E, Verotta L, Franchini C, Corbo F. 2013. Biological evaluation of hyperforin and its hydrogenated analogue on bacterial growth and biofilm production. *J Nat Prod* 76:1819-23.

112. Wu CC, Yen MH, Yang SC, Lin CN. 2008. Phloroglucinols with antioxidant activity and xanthonolignoids from the heartwood of *Hypericum geminiflorum*. *J Nat Prod* 71:1027-31.

113. Zhang N, Shi Z, Guo Y, Xie S, Qiao Y, Li X-N, Xue Y, Luo Z, Zhu H, Chen C, Hu L, Zhang Y. 2019. The absolute configurations of hyperilongenols A–C: rare 12,13-seco-spirocyclic polycyclic polyprenylated acylphloroglucinols with enolizable β,β′-tricarbonyl systems from *Hypericum longistylum* Oliv. *Organic Chemistry Frontiers* 6:1491-1502.

114. Liu YY, Ao Z, Xu QQ, Zhu DR, Chen C, Wang XB, Luo JG, Kong LY. 2019. Hyperpatulols A-I, spirocyclic acylphloroglucinol derivatives with anti-migration activities from the flowers of *Hypericum patulum*. *Bioorg Chem* 87:409-416.

115. Tanaka N, Mamemura T, Shibazaki A, Gonoi T, Kobayashi J. 2011. Yojironins E-I, prenylated acylphloroglucinols from *Hypericum yojiroanum*. *Bioorg Med Chem Lett* 21:5393-7.

116. Caldeira GI, Gouveia LP, Serrano R, Silva OD. 2022. *Hypericum* Genus as a Natural Source for Biologically Active Compounds. *Plants (Basel)* 11.

117. Li J, Liu S, Koh JJ, Zou H, Lakshminarayanan R, Bai Y, Pervushin K, Zhou L, Verma C, Beuerman RW. 2015. A novel fragment based strategy for membrane active antimicrobials against MRSA. *Biochim Biophys Acta* 1848:1023-31.

118. Phang Y, Wang X, Lu Y, Fu W, Zheng C, Xu H. 2020. Bicyclic polyprenylated acylphloroglucinols and their derivatives: structural modification, structure-activity relationship, biological activity and mechanism of action. *Eur J Med Chem* 205:112646.

119. Khan F, Tabassum N, Bamunuarachchi NI, Kim YM. 2022. Phloroglucinol and Its Derivatives: Antimicrobial Properties toward Microbial Pathogens. *J Agric Food Chem* 70:4817-4838.

120. Hudson MA, Lockless SW. 2022. Elucidating the Mechanisms of Action of Antimicrobial Agents. *mBio* 13:e0224021.

121. Caesar LK, Nogo S, Naphen CN, Cech NB. 2019. Simplify: A Mass Spectrometry Metabolomics Approach to Identify Additives and Synergists from Complex Mixtures. *Analytical Chemistry* 91:11297-11305.

122. Todd DA, Parlet CP, Crosby HA, Malone CL, Heilmann KP, Horswill AR, Cech NB. 2017. Signal Biosynthesis Inhibition with Ambuic Acid as a Strategy To Target Antibiotic-Resistant Infections. *Antimicrob Agents Chemother* 61.

123. Daniel C. Harris CAL. 2018. Quantitative chemical analysis, 9th ed. WH Freeman, New York.

124. Pluskal T, Castillo S, Villar-Briones A, Orešič M. 2010. MZmine 2: Modular framework for processing, visualizing, and analyzing mass spectrometry-based molecular profile data. *BMC Bioinform* 11:395.